Mechanistic Studies on the Dissociation of Mono- and Bimetallic 1:1 Ferric Dihydroxamate Complexes: Probing Structural Effects in Siderophore Dissociation Reactions

M. Tyler Caudle, Lawrence P. Cogswell, III, and Alvin L. Crumbliss*

Department of Chemistry, Box 90346, Duke University, Durham, North Carolina 27708-0346

Received March 9, 1994[⊗]

A pH-jump kinetic technique was used to monitor the dissociation of a series of iron(III) complexes with dihydroxamic acids $[CH_3N(OH)C(O)]_2(CH_2)_n$ having a 1:1 metal-to-ligand ratio. For the initial step involving dissociation of one hydroxamate group from each iron, the complexes with $n > 6$ exhibit a first-order dependence on proton. However, the same step exhibits second-order proton-dependent kinetics when $n < 6$. When $n = 6$, two kinetically resolvable reactions are observed, one with first-order and one with second-order dependence on proton. In every case, the spectroscopic change is consistent with a bis(hydroxamato)iron(III) complex dissociating to give a mono(hydroxamato)iron(III) complex. To explain the kinetic data, a mechanism is proposed for the initial step in the dissociation reaction, which involves a dimeric complex ($Fe_2L_2^{2+}$) with a 1:1 metal-to-ligand ratio when $n \leq 6$ and a monomeric complex (FeL^+) with a 1:1 metal-to-ligand ratio when $n \geq 6$. When $n = 6$, more complicated kinetic behavior is observed which suggests that both the monomeric and dimeric forms exist simultaneously. The dissociation rate constant for the dimeric complex ($Fe_2L_2^{2+}$) depends on n, with $k_3 = 23$, 17, and 1.6 M^{-1} s^{-1} for $n = 6$, 4, and 2, respectively. The rate-limiting dissociation rate constants k_6 for the initial step in the dissociation of the monomeric complex (FeL^+) are 0.13 and 0.38 s^{-1} for $n = 8$ and 7, respectively. The dissociation of the monomeric complex is kinetically and mechanistically consistent with the dissociation of a tetradentate form of the natural siderophore complex ferrioxamine B. The final dissociation step, involving removal of the last hydroxamate group, was found to involve a dual-path mechanism having parallel acid-dependent and acid-independent pathways. The dissociation rate constants for the final dissociation step do not vary significantly with n, though substitution of a proton for methyl on the hydroxamate nitrogen does increase the overall dissociation rate. Several significant free energy correlations exist for the dissociation of the last hydroxamate group from the iron center in (dihydroxamato)iron(III) complexes, model (monohydroxamato)-iron(III) complex, and ferrioxamine B. The free energy correlations are used to elucidate the intimate mechanism for the final dissociation reaction. The overall dissociation mechanism is discussed in terms of electrostatic effects in the dimeric complexes. The dissociation mechanisms for the monomeric complexes are discussed in terms of analogous processes occurring in the ferrioxamine B system.

Introduction

Iron is one of the biologically important first-row transition metal ions. However, the available iron is limited in aerobic systems by the ease with which the stable 3+ oxidation state hydrolyzes to give insoluble precipitates. Siderophores are potent and specific iron chelators synthesized by microorganisms for the purpose of sequestering environmental iron. A large class of siderophores have hydroxamate functional groups, which can chelate iron in a bidentate fashion (Scheme 1). A number of studies have centered on the mechanism by which siderophores or model siderophores with hydroxamate chelate groups release iron,[1-19] which is relevant to the process of cellular iron metabolism. These studies have shown that it is often energetically unfavorable for the iron to be released, due to the profound stability of siderophore complexes. Therefore, elucidation of the mechanism of iron release by siderophores is a significant problem relating to the biological chemistry of siderophores and to ligand exchange at iron(III) in general.

Scheme 1. Coordination of Fe(III) by Hydroxamic Acids

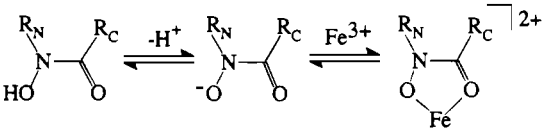

Siderophores, such as ferrioxamine B, **I**, typically have three bidentate binding sites, making them hexadentate ligands.[20,21] This is advantageous in sequestering iron(III), since a single

* To whom correspondence should be addressed.

[⊗] Abstract published in *Advance ACS Abstracts,* September 1, 1994.

(1) Matzanke, B. F.; Müller-Matzanke, G.; Raymond, K. N. In *Iron Carriers and Iron Proteins*; Loehr, T. M., Ed.; VCH Publishers, Inc.: New York, 1989; Chapter 1.
(2) Crumbliss, A. L. In *CRC Handbook of Microbial Iron Chelates*; Winkelmann, G., Ed.; CRC Press: New York, 1991; Chapter 7, pp 177–233.
(3) Monzyk, B.; Crumbliss, A. L. *J. Am. Chem. Soc.* **1979**, *101*, 6203.
(4) Brink, C. P.; Crumbliss, A. L. *Inorg. Chem.* **1984**, *23*, 4708.
(5) Biruš, M.; van Eldik, R. *Inorg. Chem.* **1991**, *30*, 4559.
(6) Biruš, M.; Bradić, Z.; Zujundžić, N.; Pribanić, M.; Wilkins, P. C.; Wilkins, R. G. *Inorg. Chem.* **1985**, *24*, 3980.
(7) Chang, C. A.; Sekhar, V. C.; Garg, B. S.; Guziec, F. S.; Russo, T. C. *Inorg. Chim. Acta* **1987**, *135*, 11.
(8) Crumbliss, A. L. *Coord. Chem. Rev.* **1990**, *105*, 155.
(9) Biruš, M.; Kujundžić, N.; Pribanić, M. *Prog. React. Kinet.* **1993**, *18*, 173.
(10) Yakirevitch, P.; Rochel, N.; Albrecht-Gary, A.; Libman, J.; Shanzer, A. *Inorg. Chem.* **1992**, *32*, 1779.
(11) Shimizu, K.; Akiyama, M. *J. Chem. Soc., Chem. Commun.* **1985**, 183.
(12) Akiyama, M.; Katoh, A.; Mutoh, T. *J. Org. Chem.* **1988**, *53*, 6089.
(13) Biruš, M.; Bradić, Z.; Krznarić, G.; Kujundžić, N.; Pribanić, M.; Wilkins, P. C.; Wilkins, R. G. *Inorg. Chem.* **1987**, *26*, 1000.
(14) Monzyk, B.; Crumbliss, A. L. *J. Am. Chem. Soc.* **1982**, *104*, 4921.
(15) Monzyk, B.; Crumbliss, A. L. *Inorg. Chim. Acta* **1981**, *55*, L5.
(16) Das, P. K.; Bhattacharya, S. G.; Banerjee, R.; Bannerjea, D. *J. Coord. Chem.* **1989**, *19*, 311.
(17) Funahashi, S.; Koji, I.; Tanaka, M. *Inorg. Chem.* **1983**, *22*, 2070.
(18) Santos, M. A.; Esteves, M. A.; Martinho, J. M. G. *J. Chem. Soc., Dalton Trans.* **1993**, 3123.
(19) Caudle, M. T.; Crumbliss, A. L. *Inorg. Chem.* **1994**, *33*, 4077.

0020-1669/94/1333-4759$04.50/0

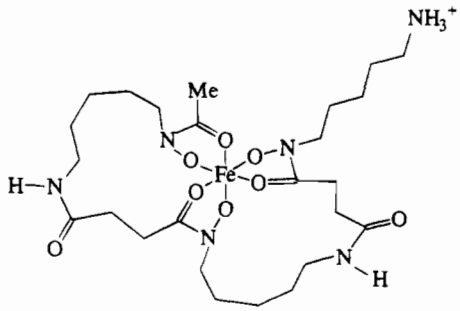

I, ferrioxamine B

hexadentate ligand can occupy all six of the available coordination sites of the metal. However, a small group of siderophores has only two hydroxamate binding sites, *i.e.* the dihydroxamic acids.[1,2,21-25] The most well-known example of a natural dihydroxamic acid is rhodotorulic acid (RA),[1,22-24] **II**, though

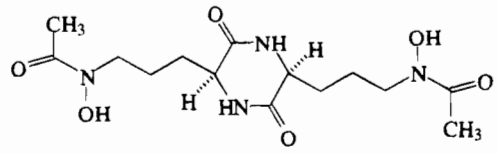

II, rhodotorulic acid (RA)

at least one other exists.[25] The unique feature of dihydroxamic acids, H_2L, is their bifunctional nature, giving them a propensity to form bimetallic complexes of stoichiometry Fe_2L_3 at pH > 3. The solution coordination chemistry of bimetallic ferric dihydroxamates has been explored.[26-35] The characteristic protonation equilibrium at excess ligand and pH > 3 is shown in eq 1. At pH < 3, further dissociation of the complex can

$$Fe_2L_3 + 2H^+ \rightleftharpoons 2FeL^+ + H_2L \quad (1)$$

$$FeL^+ + 2H^+ \rightleftharpoons Fe^{3+} + H_2L \quad (2)$$

take place according to eq 2. While Fe_2L_3 is believed to be the biologically relevant species insofar as iron transport is concerned,[1,22-25] eq 2 will be rate-limiting in the overall proton-initiated dissociation reaction due to the decreased lability of the bis(hydroxamato)iron(III) complex, FeL^+, *vs* the tris-(hydroxamato)iron(III) complex, Fe_2L_3.

It is not well understood what factors affect the energetic feasibility of ligand exchange pathways in a given siderophore system. The series of dihydroxamic acids, **III**, can function as

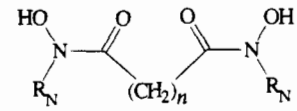

III, model dihydroxamic acids: (**a**) R_N = Me, n = 8; (**b**) R_N = Me, n = 7; (**c**) R_N = Me, n = 6; (**d**) R_N = Me, n = 4; (**e**) R_N = Me, n = 2; (**f**) R_N = H, n = 8

a direct model in the study of RA-mediated iron transport.[1,22-25] In addition, by varying the chain length n and the substituent R_N, we can probe structural influences on ligand exchange in a more general siderophore system such as ferrioxamine B, **I**.

On a more fundamental level, the ability of dihydroxamic acids to function as bridging ligands makes them useful in modeling bimetallic complexes. The bimetallic Fe_2L_3 complex has been established to exist above pH 3.[26-35] On the other hand, the ferric dihydroxamate complexes with 1:1 metal-to-ligand ratios existing at pH < 3 have been assumed to be exclusively monomeric.[26-35] However, it was recently shown by electrospray mass spectrometric measurements[36,37] that the 1:1 complex can exist as a monomer **a** or a dimer **b** (Scheme 2), depending on n. A mechanistic interpretation of kinetic data presented here is consistent with these structural assignments. Therefore, the 1:1 ferric dihydroxamates offer the unique opportunity to study the dissociation kinetics and mechanism of bimetallic complexes in an intimate way.

In this paper, we report a rigorous and extensive kinetic study on the proton-initiated dissociation of 1:1 ferric dihydroxamate complexes. We have explained the dissociation mechanism and kinetics on the basis of two factors: (1) strain in the ligand backbone upon complexation and (2) electrostatic repulsions between the two like-charged iron(III) centers in the dimeric complexes. The study of ferric dihydroxamate dissociation reactions can help elucidate electrostatic and structural factors affecting the formation and dissociation of bimetallic complexes. These results are relevant to the chemistry of siderophores, to general bimetallic complexes, and to the formation of metal-containing supramolecular assemblies.

Experimental Section

Materials and Equipment. All water used in these experiments was twice distilled, first from a solution of acidic potassium dichromate and then from basic potassium permanganate. Analytical stock solutions of 2.0 M sodium perchlorate were prepared from the solid hydrate (Aldrich 99.99%) and standardized by passing through a Dowex 50W-X8 strong-acid cation exchange column in H^+ form and titrating the liberated acid with standard base to a phenolphthalein end point. Analytical solutions of 2.0 M perchloric acid were prepared from concentrated perchloric acid (Fisher 70%) and calibrated against standard base. Analytical ferric perchlorate stock solutions were prepared from recrystallized solid ferric perchlorate hydrate and standardized for ferric ion in two ways: (1) spectrophotometrically in strong acid[38] and (2) titrimetrically by reducing with Sn(II) and titrating

(20) van der Helm, D.; Jalal, M. A. F.; Hossian, M. B. In *Iron Transport in Microbes, Plants, and Animals*; Winkelmann, G., van der Helm, D., Neilands, J. B., Eds.; VCH: Weinheim, Germany, 1987; Chapter 9.
(21) Winkelmann, G., Ed. *CRC Handbook of Microbial Iron Chelates*; CRC Press: New York, 1991.
(22) Carrano, C. J.; Raymond, K. N. *J. Bacteriol.* **1978**, *136*, 69.
(23) Müller, G.; Barclay, S. J.; Raymond, K. N. *J. Biol. Chem.* **1985**, *260*, 13916.
(24) Müller, G.; Isowa, Y.; Raymond, K. N. *J. Biol. Chem.* **1985**, *260*, 13921.
(25) Jalal, M. A. F.; Love, S. K.; van der Helm, D. *J. Inorg. Biochem.* **1986**, *28*, 417.
(26) Carrano, C. J.; Cooper, S. R.; Raymond, K. N. *J. Am. Chem. Soc.* **1979**, *101*, 599.
(27) Barclay, S. J.; Huynh, B. H.; Raymond, K. N. *Inorg. Chem.* **1984**, *23*, 2011.
(28) Barclay, S. J.; Riley, P. E.; Raymond, K. N. *Inorg. Chem.* **1984**, *23*, 2005.
(29) Das, M. K.; Chaudhury, K.; Roy, N.; Sarkar, P. *Transition Met. Chem. (New York)* **1990**, *15*, 468.
(30) Scarrow, R. C.; White, D. L.; Raymond, K. N. *J. Am. Chem. Soc.* **1985**, *107*, 6540.
(31) Santos, A. M.; Esteves, A.; Vaz, M. C. T.; Goncalves, M. L. S. S. *J. Chem. Soc., Dalton Trans.* **1993**, 927.
(32) Sun, Y.; Martell, A. E.; Motekaitis, R. *Inorg. Chem.* **1985**, *24*, 4343.
(33) Brown, D. A.; Geraty, R.; Glennon, J. D.; Choileain, N. N. *Inorg. Chem.* **1986**, *25*, 3792.
(34) Chaubet, F.; Nguyen van Duong, M.; Gref, A.; Courtieu, J.; Crumbliss, A. L.; Gaudemer, A. *Tetrahedron. Lett.* **1990**, *31*, 5729.
(35) Chaubet, F.; Duong, K. N. V.; Gref, A.; Courtieu, J.; Crumbliss, A. L.; Caudle, M. T.; Gaudemer, A. *Can. J. Chem.*, submitted for publication.
(36) Caudle, M. T.; Stevens, R. D.; Crumbliss, A. L. *Inorg. Chem.* **1994**, *33*, 843.
(37) Caudle, M. T.; Stevens, R. D.; Crumbliss, A. L. *Inorg. Chem.*, in press.
(38) Bastian, R.; Weberling, R.; Palilla, F. *Anal. Chem.* **1956**, 28, 459.

Scheme 2. Two Possible Structures for the Model 1:1 Ferric Dihydroxamate Complexes

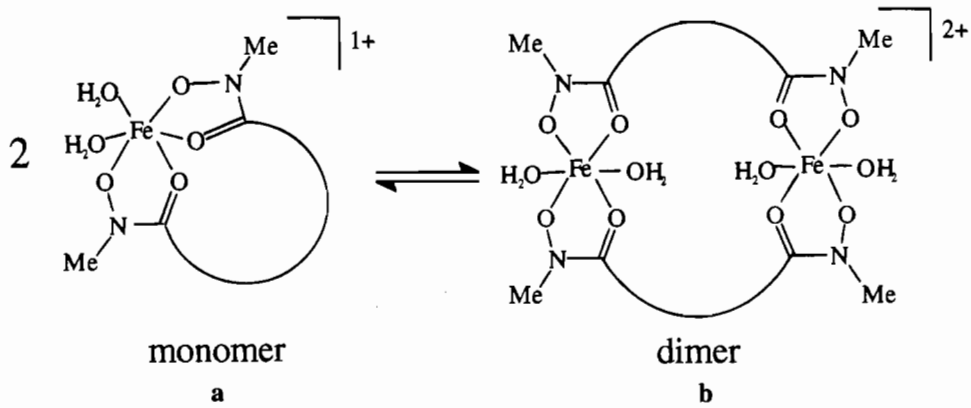

against primary standard potassium dichromate.[39] The acid concentration was determined by passing through a Dowex 50W-X8 strong acid cation exchange column in H^+ form, titrating the liberated acid, and correcting for ferric ion.

Volumetric glassware and pipet equipment were calibrated gravimetrically before use. UV/visible spectra and slow kinetics were recorded on a Hewlett-Packard 8451 diode array spectrophotometer. Rapid kinetic studies were performed on an Aminco stopped-flow mixing device equipped with a Beckman DU UV/visible monochromator for absorbance measurements and using a PC-486 based data acquisition station from On-Line Instruments. The monochromator was calibrated using the 400 nm peak of samarium perchlorate in solution to set the wavelength scale. The linearity of the photomultiplier response was checked against the absorbance of standard $KMnO_4$ solutions.

Ligand Preparation. The ligands **IIIa−e** were prepared as described in the literature[40,41] by reaction of the appropriate diacyl chloride with *N*-methylhydroxylamine in ether in the presence of aqueous sodium bicarbonate. Ligands **IIIa**, **IIIb**, and **IIIf** have been reported previously using a preparative route involving *N,N'*-carbonyldiimidazole.[33] The products were recrystallized at least twice from ethyl acetate and characterized for identity and purity by IR, NMR, MS, TLC, melting point, equivalent weight, and elemental microanalysis.

$[CH_3N(OH)C(O)]_2(CH_2)_8$, IIIa (*N,N'*-Dihydroxy-*N,N'*-dimethyldecanediamide). Anal. Found (calc): C, 55.4 (55.5); H, 9.2 (9.3); N, 10.8 (10.7). ^1H NMR: δ 1.25 (8H), 1.48 (4H), 2.30 (4H), 3.07 (6H), 9.75 (2H). IR (KBr): ν_{OH} 3150, ν_{CO} 1600 cm^{-1}. $(MH)^+$: *m/z* 261. Equiv wt found (calc): 130 (130). Mp: 106−108 °C.

$[CH_3N(OH)C(O)]_2(CH_2)_7$, IIIb (*N,N'*-Dihydroxy-*N,N'*-dimethylnonanediamide). Anal. Found (calc): C, 53.9 (53.7); H, 8.8 (8.9); N, 11.4 (11.4). ^1H NMR: δ 1.25 (6H), 1.50 (4H), 2.35 (4H), 3.10 (6H), 9.75 (2H). IR (KBr): ν_{OH} 3200, ν_{CO} 1610 cm^{-1}. $(MH)^+$: *m/z* 247. Equiv wt found (calc): 121 (123). Mp: 95−97 °C.

$[CH_3N(OH)C(O)]_2(CH_2)_6$, IIIc (*N,N'*-Dihydroxy-*N,N'*-dimethyloctanediamide). Anal. Found (calc): C, 51.7 (51.7); H, 8.8 (8.6); N, 12.0 (12.1). ^1H NMR: δ 1.28 (4H), 1.48 (4H), 2.33 (4H), 3.08 (6H), 9.78 (2H). IR (KBr): ν_{OH} 3170, ν_{CO} 1612 cm^{-1}. $(MH)^+$: *m/z* 233. Equiv wt found (calc): 116 (116). Mp: 98−100 °C.

$[CH_3N(OH)C(O)]_2(CH_2)_4$, IIId (*N,N'*-Dihydroxy-*N,N'*-dimethylhexanediamide). Anal. Found (calc): C, 47.1 (47.1); H, 7.9 (7.8); N, 13.7 (13.7). ^1H NMR: δ 1.45 (4H), 2.30 (4H), 3.05 (6H), 9.75 (2H). IR (KBr): ν_{OH} 3200, ν_{CO} 1600 cm^{-1}. $(MH)^+$: *m/z* 205. Equiv wt found (calc): 99 (102). Mp: 116−118 °C.

$[CH_3N(OH)C(O)]_2(CH_2)_2$, IIIe (*N,N'*-Dihydroxy-*N,N'*-dimethylbutanediamide). Anal. Found (calc): C, 40.9 (41.1); H, 6.9 (7.0); N, 15.9 (16.1). ^1H NMR: δ 2.50 (4H), 3.00 (6H), 9.77 (2H). IR (KBr): ν_{OH} 3200, ν_{CO} 1600 cm^{-1}. $(MH)^+$: *m/z* 177. Equiv wt found (calc): 87 (88). Mp: 122−124 °C.

IIIf was synthesized by reaction of the less reactive diester with hydroxylamine in methanol/ether in the presence of potassium hydroxide under ambient conditions. This is a modification of general ester-based syntheses for preparation of N-unsubstituted hydroxamic acids.[42,43] In the first step, 9.6 g of hydroxylamine hydrochloride (0.14 mol) was dissolved in 50 mL of boiling methanol and 11.6 g of potassium hydroxide pellets (0.207 mol) was dissolved in 30 mL of boiling methanol. The two solutions were allowed to cool to 40−50 °C and were carefully mixed with vigorous stirring and cooling in an ice bath, whereupon a white precipitate formed. When addition was complete, the solution was cooled to 0 °C and filtered to remove the precipitate. A solution of 5 mL of anhydrous methanol (0.12 mol) and 6.5 mL of pyridine (0.08 mol) in 100 mL of ether was prepared. Under nitrogen, a solution of 6.0 mL of sebacoyl dichloride (0.03 mol) in 30 mL of ether was added dropwise to the methanol/pyridine solution with vigorous stirring and cooling on ice. A white precipitate formed immediately. Upon complete reaction, the solution was allowed to stand at 0 °C and then the hygroscopic precipitate of pyridinium hydrochloride was removed by filtration. The ether solution was washed four times with 150 mL of 0.5 M sodium bicarbonate. The resulting solution of diester in ether was added to the solution of hydroxylamine with vigorous stirring. A cloudy white solution resulted almost immediately. The solution was allowed to stand at ambient temperature for several hours. It was then cooled in a dry ice bath, vacuum-filtered, and dried. To 5.3 g of this product was added 50 mL of 1.75 N acetic acid. The solution was heated to 70 °C for 10 min and then cooled in an ice bath. The solid was filtered off, washed with ether, and dried *in vacuo*. The product was recrystallized from methanol and characterized as above.

$[HN(OH)C(O)]_2(CH_2)_8$, IIIf (*N,N'*-Dihydroxydecanediamide). Anal. Found (calc): C, 51.7 (51.7); H, 8.5 (8.7); N, 11.9 (12.1). ^1H NMR: δ 1.50 (8H), 1.70 (4H), 2.20 (4H), 8.95 (2H), 10.60 (2H). IR (KBr): ν_{NH} 3253, ν_{OH} 2720−3360, ν_{CO} 1624 cm^{-1}. $(MH)^+$: *m/z* 233. Equiv wt found (calc): 117 (116). Mp: 161 °C dec.

Equilibrium and Kinetic Measurements. Rapid dissociation kinetics were measured on the stopped-flow apparatus by a pH-jump kinetic method. Equal volumes of a solution containing the fully-formed 1:1 iron(III) dihydroxamate complex at pH $\approx$ 2 and one containing a precisely known quantity of excess perchloric acid were mixed, and the absorbance change was monitored with time up to 300 s. The slow final dissociation step was monitored in the stopped-flow regime by an initial-rate method over a maximum time scale of 300 s. The full absorbance decay of the final step was monitored with slow manual mixing in the HP 8451 spectrophotometer up to a maximum time of 30 min. Kinetic data points in the figures represent an average of three to six kinetic runs. Approximate uncertainties are reflected by the size of the data points or error bars. Uncertainties in kinetic and equilibrium parameters are quoted as 90% confidence limits.

Final equilibrium solution spectra were collected 5−30 min after mixing at various acidities, $[H^+] = 0.02-1.0$ M. The spectrophotometric data were analyzed to determine relevant equilibrium constants

(39) Vogel, A. I. *Quantitative Inorganic Analysis Including Elementary Instrumental Analysis*, 3rd ed.; Longmans, Green and Co., Ltd.: London, 1968.
(40) Smith, W. L.; Raymond, K. N. *J. Am. Chem. Soc.* **1980**, *102*, 1252.
(41) Das, M. K.; Bose, P.; Roy, N. *J. Chem. Eng. Data* **1984**, *29*, 345.
(42) Hauser, C. R.; Renfrow, W. B. *Org. Synth.* **1943**, *2*, 67.
(43) Hurd, C. D.; Botteron, D. G. *J. Org. Chem.* **1946**, *11*, 207.

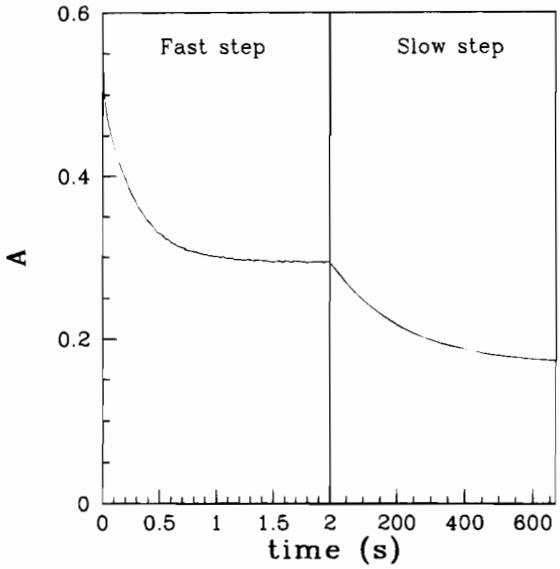

Figure 1. Absorbance decay data for the pH-jump dissociation of the iron(III) complex with **IIIc**. $[Fe^{3+}]_{tot} = [L^{2-}]_{tot} = 0.30$ mM. $[H^+] = 0.500$ M. $I = 2.0$ M ($NaClO_4/HClO_4$). $T = 25$ °C. $\lambda = 470$ nm.

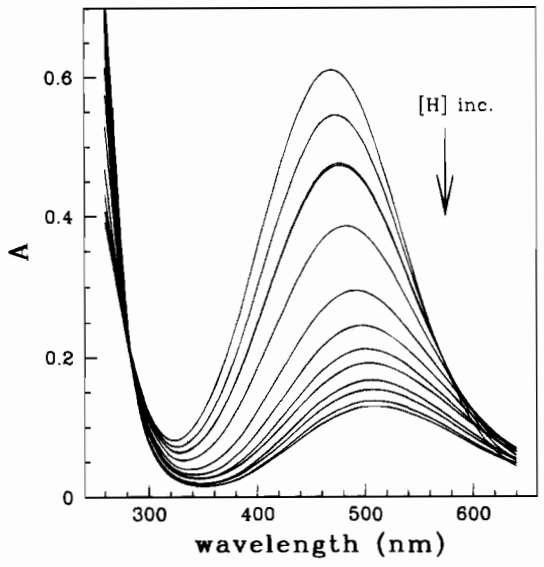

Figure 2. Solution spectra of the iron(III) complex with **IIIc** at various $[H^+]$ measured at final equilibrium. $[Fe^{3+}]_{tot} = [L^{2-}]_{tot} = 0.30$ mM. $I = 2.0$ M ($NaClO_4/HClO_4$). $T = 25$ °C. $[H^+] = 0.020-0.900$ M.

using the program SQUAD.[44,45] Intermediate quasi-equilibrium spectra were collected no later than 5.0 min after mixing, depending on the rate of the fast dissociation reaction under observation.

Results

General Observations. The pH-jump absorbance-decay data (Figure 1) for a representative ferric dihydroxamate having a 1:1 metal-to-ligand ratio illustrate that the overall dissociation reaction, eq 2, occurs in two distinct kinetic steps whose time scales are separated by several orders of magnitude. It is, therefore, useful to present the kinetic and mechanistic analysis for the dissociation reaction, eq 2, in two parts as well. For purposes of clarity, the two steps will be referred to by their time scales as the "fast" step and the "slow" step.

All pH-jump reactions were performed under pseudo-first-order conditions of excess proton. In the time regime over which the fast step occurs, a complex series of dissociation reactions is observed. The number of reaction substeps involved in the fast step varies with the ligand, and the trend is not immediately straightforward. Therefore, a detailed kinetic treatment of each iron(III) dihydroxamate system (H_2L = **IIIa**–**f**) is presented below. In a qualitative sense, one or more first-order absorbance decays are observed for each system. The spectroscopic change involved in the fast step is associated with dissociation of one hydroxamate group from a bis(hydroxamato)iron(III) complex ($\lambda_{max} = 470$ nm) to give the protonated mono(hydroxamato)iron(III) complex ($\lambda_{max} = 505$ nm). However, the reaction order with respect to proton shifts from first-order for $n \geq 6$ to second-order for $n \leq 6$. Interestingly, both first-order and second-order proton-dependent reactions are observed when $n = 6$. Therefore the iron(III) complex with **IIIc** appears to be a system in which some fundamental change in structure occurs, which is dependent on the chain length separating the hydroxamate sites.

On the time scale over which the slow step is monitored, only a single dissociation reaction can be observed. Under the same pseudo-first-order conditions of excess proton, a first-order absorbance decay is observed. The spectroscopic change is associated with removal of the final hydroxamate group from the mono(hydroxamato)iron(III) complex to yield free iron and free ligand in solution. The slow-step dissociation rates show no significant dependence on the chain length n but do show a strong dependence on the nature of the substituent at R_N, **III**, as expected.[3,4,19,46]

Final Equilibrium Spectra. Solution spectra of a representative 1:1 ferric dihydroxamate (Figure 2) show the equilibrium spectroscopic dependence on $[H^+]$. The most intense spectrum ($[H^+] = 0.020$ M, λ_{max} 470 nm) is consistent with a bis(hydroxamato)iron(III) complex at low acidity.[1-19,26-33] As $[H^+]$ is increased to as high as 1.0 M, the spectrum shows a decrease in intensity and a shift toward longer wavelength. This is characteristic of the stepwise dissociation of an aqueous bis(hydroxamato)iron(III) complex, where a stable mono(hydroxamato)iron(III) intermediate is formed.[6,13,14,27,47] There is no single isosbestic point encompassing all of the spectra, indicating that more than two iron(III) species exist in solution over this pH range. Matrix rank analysis of the absorbance spectra[48,49] was used to estimate the number of iron(III) species existing in the range $[H^+] = 0.02-1.0$ M. For an absorbance error[48,49] of 0.0005 unit, a rank of 3 was determined for the absorbance matrix, suggesting that three stable species exist in solution over this acidity range. Species stoichiometry was selected on the basis of kinetic results (below) and from a rigorous analysis of the equilibrium spectrum (Figure 2) for each complex to find the model giving the best fit to the spectra. The equilibrium constants were determined by fitting the equilibrium model based on the proposed reaction mechanism (Scheme 3) to the equilibrium spectra and are listed in Table 1. Equilibrium constants involving less stable species were estimated from kinetic parameters and are noted as such in Table 1.

Fast-Step Dissociation Kinetics. The absorbance spectra of the iron(III) complex with **IIIc** at various acid concentrations (Figure 3 (inset)) were measured a few seconds after pH-jump mixing. These spectra correspond, therefore, to a quasi-equilibrium position in the dissociation reaction where the fast

(44) Leggett, D. J. Stability Quotients from Absorbance Data. In *Computational Methods for the Determination of Formation Constants*; Leggett, D. J., Ed.; Plenum Press: New York, 1985; Chapter 6.
(45) Leggett, D. J. *Anal. Chem.* **1977**, *49*, 276.
(46) Fish, L. L.; Crumbliss, A. L. *Inorg. Chem.* **1985**, *24*, 2198.
(47) Biruš, M.; Kujundžić, N.; Pribanić, M. *Croat. Chem. Acta* **1984**, *57*, 313.
(48) Meloun, M. J. H.; Högfeldt, E. *Computation of Solution Equilibria*; John Wiley & Sons: New York, 1988.
(49) Wallace, R. M.; Katz, S. M. *J. Phys. Chem.* **1964**, *68*, 3890.

Table 1. Equilibrium Parameters Defined in Scheme 3 for Dissociation of (Dihydroxamato)iron(III) Complexes[a]

ligand	10^4K_1[b]	K_2[c,d]	K_3[e]	K_4[c,f]	K_5[c,g]	K_6[g]
IIIa	0.2(2)	11(11)			1.6(2)	7(7)
IIIb	2(1)	7(3)			1.1(2)	6(2)
IIIc	7(2)	≈20[h]	0.016(2)	0.8(1)		
IIId	7.8(5)		0.034(3)	0.94(8)		
IIIe	12(2)		0.010(3)	0.6(2)		
IIIf	170(35)	1.3(2)[i]				

[a] $[Fe^{3+}]_{tot} = [L^{2-}]_{tot} = 0.30$ mM. $I = 2.0$ M ($NaClO_4/HClO_4$). $T = 25$ °C. Uncertainties quoted are 90% confidence limits. [b] From equilibrium spectrum analysis of the slow step. [c] M^{-1}. [d] $K_2 = K_5K_6$. [e] From equilibrium spectrum analysis and K_4. [f] From analysis of kinetic data for the fast step, eq 13. [g] From kinetic parameters. $K = k_f/k_r$. [h] Estimated. [i] Path 2 only. No values available for K_5 and K_6.

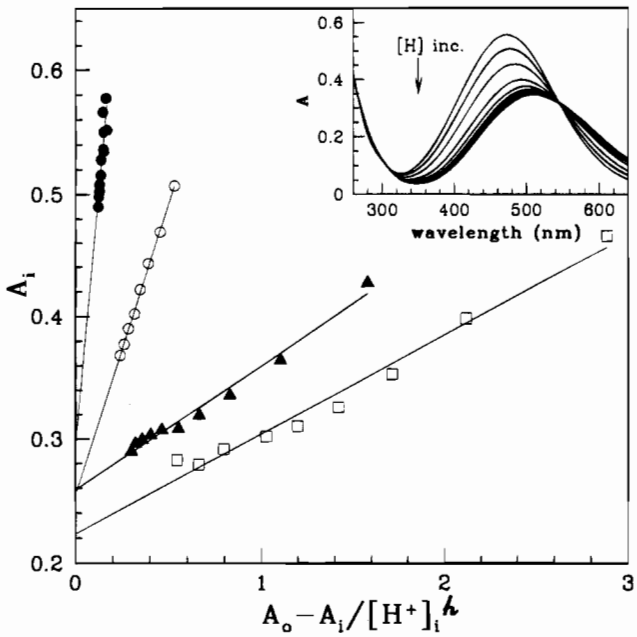

Figure 3. Absorbance data at 470 nm measured after equilibration of the fast step and plotted according to eq 3: (●) H_2L = **IIIa**; (○) H_2L = **IIIb**; (▲) H_2L = **IIIc**; (□) H_2L = **IIId**. $[Fe^{3+}]_{tot} = [L^{2-}]_{tot} = 0.30$ mM. $I = 2.0$ M ($NaClO_4/HClO_4$). $T = 25$ °C. $\lambda = 470$ nm. For all data, $h = 1$. Inset: Absorbance spectra of the Fe(III) complex with **IIIc** at various $[H^+]$ measured immediately after equilibration of the fast step. $[H^+] = 0.10 - 1.00$ M.

step has just equilibrated but the slow step has not proceeded to any significant degree. Replacing **IIIc** with another of the dihydroxamate ligands does not change the general shape of the spectrum or the trend with respect to $[H^+]$, though the total absorbance change for a given $[H^+]$ does vary with ligand.

At 470 nm, λ_{max} for the bis(hydroxamato)iron(III) complex, there is a decrease in absorbance with increasing $[H^+]$. A sharp isosbestic point is observed, and rank analysis of the absorbance matrix[48,49] confirms the presence of only two complexes. More rigorous analysis of the spectra was performed by the SQUAD[44] algorithm, which allows for deconvolution of a series of concentration-dependent spectra into absorptivity spectra of individual species. The acid-dependent removal of one hydroxamate group from a bis(hydroxamato)iron(III) center was found to be the model best fitting the spectroscopic data for all of the iron(III) complexes of **IIIa**–**f** (Figure 3 (inset)).[6,13,14,27,47] However, it is important to note that the acid-dependent absorbance data for *all* of the complexes could be equally well fit by assuming either the monomeric or the dimeric structure for the 1:1 complex (Scheme 2).

The proton stoichiometry for the fast acid-dependent dissociation reaction was determined by plotting the equilibrium absorbance data at 470 nm (Figure 3 (inset)), as a function of $[H^+]$ in the form of a Schwarzenbach plot[50,51] (Figure 3) according to eq 3. The Schwarzenbach plot was used to

$$A_i = \frac{A_0 - A_i}{K_H[H^+]_i^h} + A_f \qquad (3)$$

A_i = observed absorbance at $[H^+]_i$

A_0 = initial absorbance (of unprotonated species)

A_f = final absorbance (of protonated species)

determine the number of protons involved in the dissociation reaction since a plot of A_i *vs* $(A_i - A_0)/[H^+]_i^h$ is linear only for the correct value of h, the number of protons transferred. The linear plots in Figure 3 were obtained for an integral h value of 1. Only the iron complexes with **IIIa**–**d** gave absorbance spectra suitable for this analysis.

Ligands IIIa and IIIb. For the iron(III) complexes with **IIIa,b**, the fast step exhibits two first-order absorbance decays (Figure 4a) over the appropriate time regime. The acid-dependent pseudo-first-order rate constants for the first step, k_5^{exp}, were determined by numerically fitting a single-exponential decay, eq 4, to the absorbance decay curve observed over

$$A - A_\infty = Be^{-kt} \qquad (4)$$

a 0.3 s time scale. For the iron(III) **IIIa,b** complexes, k_5^{exp} exhibits a linear dependence on $[H^+]$ (Figure 4b), suggesting a reaction first-order in proton. There is no dependence on the initial concentration of the complex provided $[Fe^{3+}]_{tot} = [L^{2-}]_{tot}$. There is an increase in k_5^{exp} when the ligand is in excess over the iron. This is likely due to formation of higher complex species and was not explored further.

The slower absorbance decay associated with k_6^{exp} in Figure 4a overlaps the absorbance decay due to the final slow step. This results in the "tailing off" of the absorbance decay in Figure 4a. This reaction must, therefore, be analyzed as a biphasic system. The acid-dependent pseudo-first-order rate constant, k_6^{exp}, was determined by fitting a two-exponential decay, eq 5,

$$A - A_\infty = Be^{-k(1)t} + Ce^{-k(2)t} \qquad (5)$$

to the absorbance decay data on a 90 s time scale. Under these conditions, the slower reaction is far from complete, but an acceptable fit and reasonable values for k_6^{exp} were obtained. Saturation-like kinetics with respect to $[H^+]$ are exhibited by k_6^{exp} (Figure 4c). This is consistent with a proton-independent reaction which is preceded on the reaction coordinate by a rapidly established proton-dependent equilibrium.

The reaction sequence in eqs 6 and 7 is consistent with the data presented in Figure 4. The fact that only one proton is

$$FeL^+ + H^+ \rightleftharpoons FeLH'^{2+} \qquad k_5, k_{-5}, K_5 \qquad (6)$$

$$FeLH'^{2+} \rightleftharpoons FeLH^{2+} \qquad k_6, k_{-6} \qquad (7)$$

transferred in eqs 6 and 7 is also consistent with Figure 3, which established a single-proton dependence for the overall fast step. From eq 6, a linear expression for k_5^{exp} as a function of $[H^+]$

(50) Raymond, K. N.; Müller, G.; Matzanke, B. F. *Top. Curr. Chem.* **1984**, *123*, 49.
(51) Anderegg, G.; L'Eplattenier, F.; Schwarzenbach, G. *Helv. Chim. Acta* **1963**, *46*, 1409.

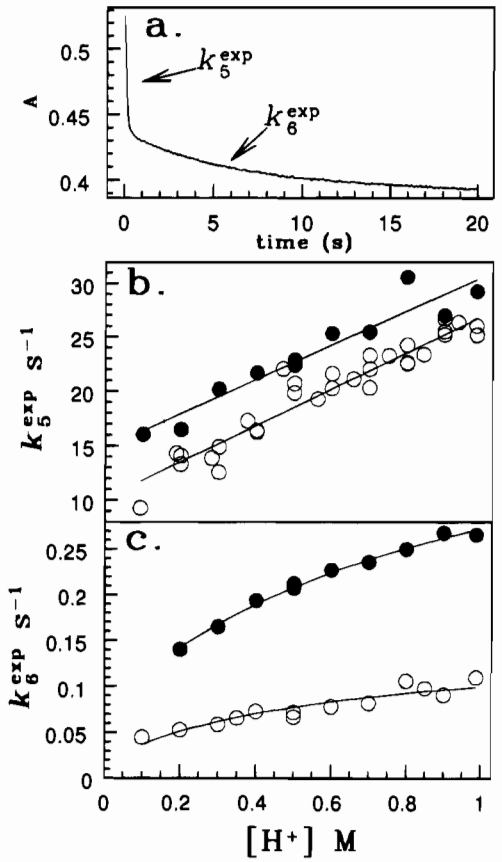

Figure 4. Kinetic data for the fast step in the pH-jump dissociation of the iron(III) complexes with **IIIa** and **IIIb**: (○) H_2L = **IIIa**; (●) H_2L = **IIIb**. $[Fe^{3+}]_{tot} = [L^{2-}]_{tot} = 0.30$ mM. $I = 2.0$ M ($NaClO_4/HClO_4$). $T = 25$ °C. $\lambda = 470$ nm. (a) Absorbance decay data showing the time region used to determine k_5^{exp} and k_6^{exp}. H_2L = **IIIb**. $[H^+] = 0.500$ M. (b) k_5^{exp} *vs* $[H^+]$. Data were analyzed using $k_5^{exp} = a[H^+] + b$. **IIIa**, $a = 17(1)$ M^{-1} s^{-1}, $b = 10(1)$ s^{-1}, $s_y = 1.4$, $r^2 = 0.96$; **IIIb**, $a = 16(3)$ M^{-1} s^{-1}, $b = 15(2)$ s^{-1}, $s_y = 1.5$, $r^2 = 0.96$. (c) k_6^{exp} *vs* $[H^+]$. Data were analyzed using $k_6^{exp} = a[H^+]/(b[H^+] + 1) + c$. **IIIa**, $a = 0.21(6)$ M^{-1} s^{-1}, $b = 1.64$ M^{-1} (fixed), $c = 0.02(2)$ s^{-1}; **IIIb**, $a = 0.41(6)$ M^{-1} s^{-1}, $b = 1.07$ M^{-1} (fixed), $c = 0.08(2)$ s^{-1}. Uncertainties quoted are 90% confidence limits.

can be derived:

$$k_5^{exp} = k_5[H^+] + k_{-5} \quad (8)$$

Equation 8 was used to determine the microscopic rate constants k_5 and k_{-5} (Table 2) from the slopes and intercepts, respectively, of Figure 4b. The overall reaction, eqs 6 and 7, was used to derive an expression, eq 9, that is consistent with saturation in

$$k_6^{exp} = \frac{k_6K_5[H^+]}{1 + K_5[H^+]} + k_{-6} \quad (9)$$

the $[H^+]$ dependence observed in Figure 4c. The parameters in eq 9 gave the values of k_6, k_{-6}, and K_5 (Tables 1 and 2) when fit to the data in Figure 4c.

Ligands IIId and IIIe. A single first-order absorbance decay is associated with the fast step in the pH-jump dissociation of the complexes of iron(III) with **IIId** or **IIIe**. The acid-dependent pseudo-first-order rate constants, k_3^{exp}, were determined by fitting a single-exponential decay, eq 4, to the absorbance decay data on a 30 s time scale. The nonlinear dependence of k_3^{exp} on $[H^+]$ (Figure 5) suggests a reaction second-order in proton. This appears to be inconsistent with the equilibrium data in Figure 3, which established that, for dissociation of the iron complex

Table 2. Microscopic Kinetic Parameters Defined in Scheme 3 for the Initial Step in the Dissociation of (Dihydroxamato)iron(III) Complexes[a]

ligand	k_2[b]	k_{-2}[c]	k_3[b]	10^2k_{-3}[b,d]	k_5[b]	k_{-5}[c]	k_6[c]	k_{-6}[c]
IIIa					17(2)	10(1)	0.13(4)	0.02(2)
IIIb					16(3)	15(2)	0.38(6)	0.08(2)
IIIc	200(20)		23(3)	14(3)				
IIId			17(2)	5.0(8)				
IIIe			1.6(6)	1.6(8)				
IIIf	83(9)	62(6)						

[a] $[Fe^{3+}]_{tot} = [L^{2-}]_{tot} = 0.30$ mM. $I = 2.0$ M ($NaClO_4/HClO_4$). $T = 25$ °C. Uncertainties quoted are 90% confidence limits. [b] M^{-1} s^{-1}. [c] s^{-1}. [d] Calculated from equilibrium data, $K = k_f/k_r$.

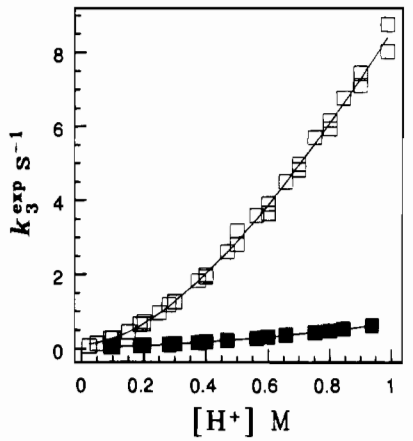

Figure 5. Kinetic data for the fast step in the pH-jump dissociation of the iron(III) complexes with **IIId** and **IIIe**. $[Fe^{3+}]_{tot} = [L^{2-}]_{tot} = 0.30$ mM. $I = 2.0$ M ($NaClO_4/HClO_4$). $T = 25$ °C. $\lambda = 470$ nm. Data were analyzed using $k_3^{exp} = a[H^+]^2/(1 + b[H^+]) + c$. Key: (□) H_2L = **IIId**, $a = 16.4(8)$ M^{-1} s^{-1}, $b = 0.94(8)$ M^{-1}, $c = 0.12(6)$ s^{-1}; (■) H_2L = **IIIe**, $a = 1.0(3)$ M^{-1} s^{-1}, $b = 0.6(2)$ M^{-1}, $c = 0.04(2)$ s^{-1}. Uncertainties quoted are 90% confidence limits.

with **IIId**, a single proton is transferred. However, if we consider the possibility of the dimeric structure in Scheme 2, then these two apparently contradictory observations can be resolved.

We expect the dependence of the absorption spectra (per iron center) on the protonation state of the iron complex to be identical for **a** and **b** in Scheme 2, since the two protonation sites are identical.[52] Therefore, the data in Figure 3, which illustrate the spectrophotometric dependence on $[H^+]$ per iron chromophore, will be linear with $h = 1$ for either **a** or **b** (Scheme 2). In other words, the spectra cannot distinguish between the monomeric and dimeric structures. On the other hand, the kinetic data in Figure 5 measure the proton dependence per reacting molecule, which is found to be second-order in $[H^+]$. The most reasonable way to account for both data sets is to propose a ground state containing two identical iron protonation sites which reacts *via* a simultaneous two-proton transfer.

The data shown in Figures 3 and 5 are then consistent with the scheme

$$Fe_2L_2^{2+} + H^+ \rightleftharpoons Fe_2L_2H^{3+} \quad K_4 \quad (10)$$

$$Fe_2L_2H^{3+} + H^+ \rightleftharpoons 2FeLH^{2+} \quad k_3, k_{-3} \quad (11)$$

Equation 12 gives the full second-order differential rate equation corresponding to eqs 10 and 11. $[Fe^{3+}]_{tot}$ is the total iron(III) concentration. Since we observe first-order kinetics for these reactions, we assume relaxation conditions hold for eq 12. An

(52) See paragraph at end of paper regarding supplementary material.

$$\frac{d[FeLH^{2+}]}{dt} = \frac{k_3K_4[H^+]^2}{1 + K_4[H^+]}([Fe^{3+}]_{tot} - [FeLH^{2+}]) - 2k_{-3}[FeLH^{2+}]^2 \quad (12)$$

approximate first-order expression can then be derived from eq 12, in which the macroscopic first-order relaxation constant k_3^{exp} is given by

$$k_3^{exp} = \frac{k_3K_4[H^+]^2}{1 + K_4[H^+]} + 2k_{-3}[FeLH^{2+}]_{eq} \quad (13)$$

Equation 13 gave an excellent fit to the data in Figure 5, and the fitting parameters were used to determine k_3 and K_4 (Tables 1 and 2). The rate constant k_{-3} could not be determined from eq 13 with any precision, since the intercept in Figure 5 is statistically small. Therefore, k_{-3} was determined from equilibrium parameters by the relationship $k_{-3} = k_3/K_3$ (Table 2). The equilibrium constant K_3 was determined from an analysis of the spectra collected after the final equilibrium (Table 1).

Ligand IIIc. The pH-jump data for the fast step in the dissociation of the iron(III) complex with **IIIc** exhibit two first-order absorbance decays (Figure 6a). In contrast to that of Figure 4, however, the acid dependence is not consistent with eqs 6 and 7. The first decay, corresponding to a pseudo-first-order rate constant k_2^{exp}, is more than an order of magnitude more rapid than the second (Figure 6a). However, because of difficulties in sufficiently resolving the two steps over the entire $[H^+]$ range studied, a biphasic absorbance decay, eq 5, was fit to the absorbance decay data on a time scale of up to 30 s. In this way, k_2^{exp} and k_3^{exp} were determined simultaneously. The rate constant, k_2^{exp}, is dependent on $[H^+]$ in a nominally linear way (Figure 6b), though there is significant scatter in the data. The linear dependence suggests a reaction that is first-order in proton. A second-order proton dependence is observed for k_3^{exp} (Figure 6c), similar to that observed for the iron complexes of **IIId** and **IIIe**. This would, again, appear to contradict the data in Figure 3 unless this reaction involves a bimetallic complex with two identical protonation sites (Scheme 2, **b**).

The data in Figure 6 are consistent with a parallel scheme in which two different reactants dissociate to give the same products. By one pathway, the monomeric complex, FeL^+, dissociates *via* a first-order proton-dependent mechanism, eq 14. A straight line was fit to the data in Figure 6b, as suggested

$$FeL^+ + H^+ \rightleftharpoons FeLH^{2+} \qquad k_2, k_{-2}, K_2 \quad (14)$$

by the rate law for eq 14, to determine k_2 and k_{-2} (Table 2)

$$k_2^{exp} = k_2[H^+] + k_{-2} \quad (15)$$

In the parallel pathway, the dimeric complex $Fe_2L_2^{2+}$ dissociates *via* a two-proton mechanism, eqs 10 and 11. An excellent fit of eq 13 to Figure 6c was obtained, and the fitting parameters were used to compute k_3 and K_4 (Tables 1 and 2). This implies that, for the **IIIc** ligand, both the monomeric and dimeric iron complexes exist simultaneously in solution at the beginning of the reaction, which is consistent with independent electrospray mass spectrometric experiments.[36,37]

Ligand IIIf. The fast step in the dissociation of the iron complex with **IIIf** occurs in a single step. Equation 4 was fit to the pH-jump absorbance decay data to determine the pseudo-first-order rate constants, k_2^{exp}, for this system. For $[H^+]$ values of 0.200, 0.300, 0.408, 0.600, 0.700, 0.800, 0.900, and 0.988 M, k_2^{exp} is 82.25, 85.61, 89.94, 110.1, 124.4, 128.1, 134.9, and 143.8 s^{-1}. A linear relationship exists between k_2^{exp} and $[H^+]$, $r^2 = 0.99$, suggesting a first-order proton dependence, eq 14. A linear fit of eq 15 to the pseudo-first-order rate constant data gave k_2 and k_{-2} (Table 2).

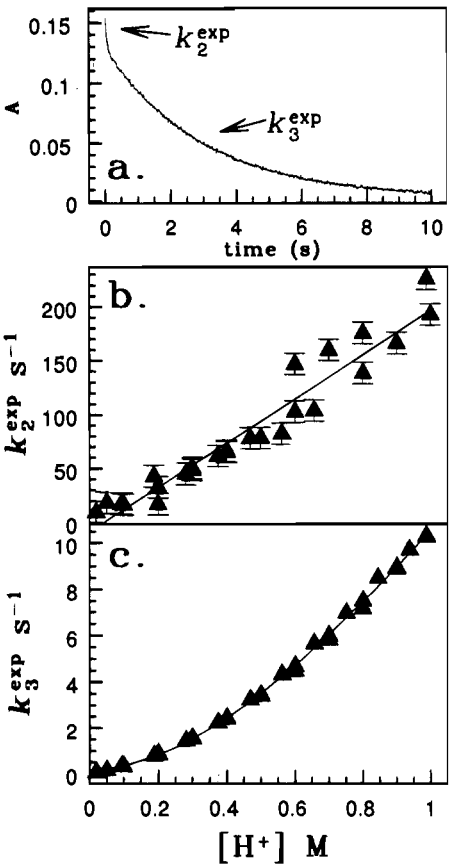

Figure 6. Kinetic data for the fast step in the pH-jump dissociation of the iron(III) complex with **IIIc**. $[Fe^{3+}]_{tot} = [L^{2-}]_{tot} = 0.30$ mM. $I = 2.0$ M ($NaClO_4/HClO_4$). $T = 25$ °C. $\lambda = 470$ nm. (a) Absorbance decay data showing the time region used to determine k_2^{exp} and k_3^{exp}. (b) k_2^{exp} *vs* $[H^+]$. Data were analyzed using $k_2^{exp} = a[H^+] + b$. $a = 2.0(2) \times 10^2$ M^{-1} s^{-1}, $b = -9(11)$ s^{-1}, $s_y = 16$, $r^2 = 0.97$. (c) k_3^{exp} *vs* $[H^+]$. Data were analyzed using $k_3^{exp} = a[H^+]^2/(1 + b[H^+]) + c$. $a = 18(1)$ M^{-1} s^{-1}, $b = 0.8(1)$ M^{-1}, $c = 0.2(1)$ s^{-1}. Uncertainties quoted are 90% confidence limits.

Mechanism of the Fast Step. The kinetic and equilibrium data for the fast step (Tables 1 and 2) are consistent with Scheme 3. Path 1 is operative for the ligands **IIIa,b**, and path 2 is operative for **IIIc,f**. Paths 1 and 2 exist, therefore, for those ligands with the longest connecting chains. Path 3 is operative for those ligands with the shortest connecting chains, **IIIc−e**. Both paths 2 and 3 are proposed to exist for **IIIc**. The implication is that there is a shift in the structure of the fully formed complex from monomeric to dimeric (Scheme 2) as n decreases. This is in complete agreement with electrospray mass spectrometric results showing that, at pH = 2, the ferric dihydroxamates in this study form the dimer for $n \leq 6$ but the monomer for $n \geq 6$.[36,37]

The dissociation of $Fe_2L_2^{2+}$ to give the bidentate complex $FeLH^{2+}$ is proposed to occur in two steps (Scheme 3 (path 3)). The first is a rapidly established proton-dependent equilibrium with an equilibrium constant K_4. This intermediate $Fe_2L_2H^{3+}$ is not observed as a stable species, thermodynamically or kinetically. In spectra taken after equilibration of the fast step in the dissociation of the dimeric complexes with **IIIc−e** (Figure 3 (inset)), only two species were observed at equilibrium. Furthermore, only a single kinetic step was observed in the fast step of the dissociation of iron(III) complexes with **IIId** and

Scheme 3. Reaction Scheme for the Overall Dissociation of Iron(III) Complexes with **IIIa−f**

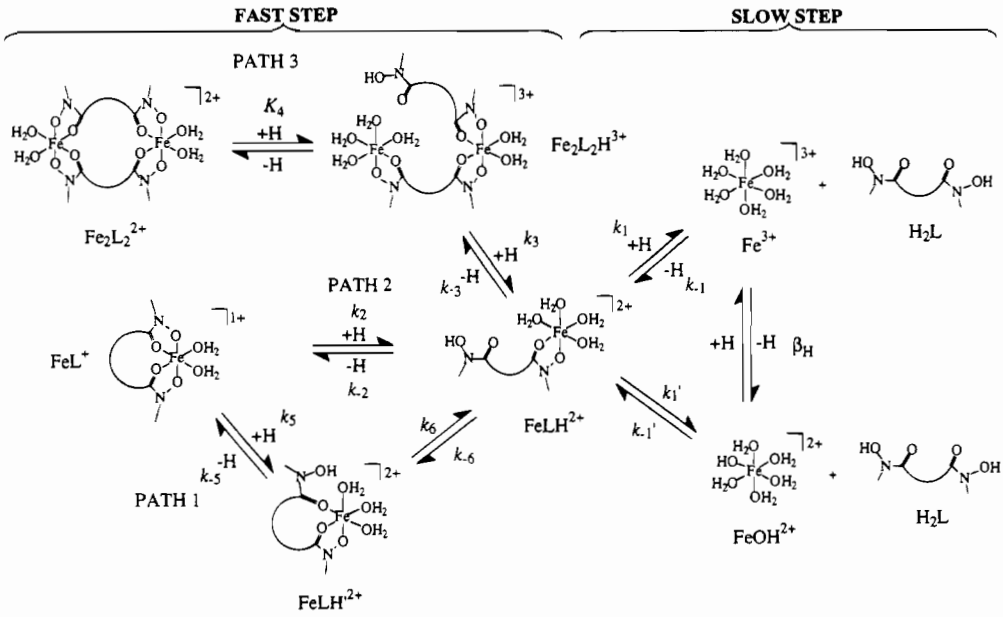

IIIe, indicating that $Fe_2L_2H^{3+}$ is not a kinetically stable intermediate. However, a rate law assuming a single two-proton step did not adequately fit the kinetic data for **IIIc−e** in Figures 5 and 6, so $Fe_2L_2H^{3+}$ was proposed to exist as an unstable intermediate in the dissociation of the dimeric complexes. Using the equilibrium constants K_4, speciation calculations showed that, over the accessible $[H^+]$ range, $Fe_2L_2H^{3+}$ does not exist in significant (observable) quantities at equilibrium.

Slow-Step Dissociation Kinetics. The final dissociation step can be observed if the pH-jump absorbance decay curve is monitored on a time scale up to 30 min (Figure 1). The first-order absorbance decay at 470 and 510 nm is associated with dissociation of a bidentate mono(hydroxamato)iron(III) complex to give free hydrated iron(III) and the protonated ligand. The kinetic data for the slow step is consistent with the general dual-path mechanism for dissociation of mono(hydroxamoto)iron-(III) complexes for all of the dihydroxamate ligands studied, eqs 16−18. Since the rate of the slow step is several orders of

$$FeLH^{2+} + H^+ \rightleftharpoons Fe^{3+} + H_2L \qquad k_1, k_{-1} \tag{16}$$

$$FeLH^{2+} \rightleftharpoons FeOH^{2+} + H_2L \qquad k_1', k_{-1}' \tag{17}$$

$$Fe^{3+} \rightleftharpoons FeOH^{2+} + H^+ \qquad \beta_H \tag{18}$$

magnitude slower than that of the fast step at the same $[H^+]$, reactions occurring as part of the fast step (Scheme 3) can be regarded as pre-equilibrium steps in the analysis of the slow step.

Ligands IIIa−d. The pseudo-first-order rate constant, k_1^{exp}, was somewhat irreproducible when the full absorbance decay curve was analyzed. Furthermore, accounting for all of the pre-equilibrium steps led to complicated expressions for the $[H^+]$ dependence of the pseudo-first-order rate constant which were not useful in determining the microscopic rate constants for the system. Consequently, initial rate studies were performed on the iron(III) complexes with **IIIa−d**.

According to eqs 16 and 17, the initial rate for the loss of $FeLH^{2+}$ is given by eq 19. The relationship between $[FeLH^{2+}]_{t=0}$

$$\left(\frac{d[FeLH^{2+}]}{dt}\right)_{t=0} = -(k_1[H^+] + k_1')[FeLH^{2+}]_{t=0} \tag{19}$$

and the absorbance measurements is not straightforward. However, the pre-equilibrium constants K_s are known from the kinetic studies on the fast dissociation reaction (Table 1). It is possible, therefore, to calculate the initial absorbance of the solution and relate $(d[FeLH^{2+}]/dt)_{t=0}$ to the measured initial rate, $(dA/dt)_{t=0}$, in terms of absorbance units. By a process of linearization, a function q can be derived,[52] which leads to a simple expression, eq 20, for the forward microscopic rate

$$q = k_1[H^+] + k_1' \tag{20}$$

constants k_1 and k_1'. The precise analytical expression for q depends on the nature of the pre-equilibrium, Scheme 3.

A plot of q *vs* $[H^+]$ is linear for all of the data in Figure 7, corresponding to the iron complexes with **IIIa−d**. From a fit of eq 20 to the data in Figure 7, the values of k_1 and k_1' were obtained (Table 3). The reverse rate parameters, k_{-1} and k_{-1}', were determined from equilibrium data. Reasonably accurate values for the equilibrium constants K_{2-6} for the fast step (Table 1) are required to have confidence in the values of k_1 and k_1'. This is somewhat problematic for the iron(III) complex with **IIIc**, since a precise value for K_2 could not be obtained. K_2 was estimated to be 20, a reasonable value based on the fit of eq 20 to the initial-rate kinetic data. A further difficulty with the **IIIc** system is the complexity of the function q when both paths 2 and 3 in Scheme 3 are operative. While a nominally linear plot results from analysis of these data, the accuracy of k_1 and k_1' is less certain for this system.

Ligands IIIe and IIIf. Contrary to those with ligands **IIIa−d**, the iron(III) complexes with **IIIe** and **IIIf** yield more reproducible k_1^{exp} values, and the fast and slow dissociation steps go nearly to completion under the conditions employed. This greatly simplifies the analytical expression for the proton dependence of k_1^{exp} and, therefore, the determination of the microscopic rate constants. The pseudo-first-order rate constant shows a nominally linear dependence on $[H^+]$ for the iron complex with **IIIe** (Figure 8a), though the scatter is fairly large. The data for **IIIf** in Figure 8b show a slight nonlinearity in the $[H^+]$ dependence but considerably less scatter.

Since the fast pre-equilibrium step goes to completion, the rate law is simply analogous to that derived for dissociation of mono(hydroxamato)iron(III) complexes.[3,4,46] The expression

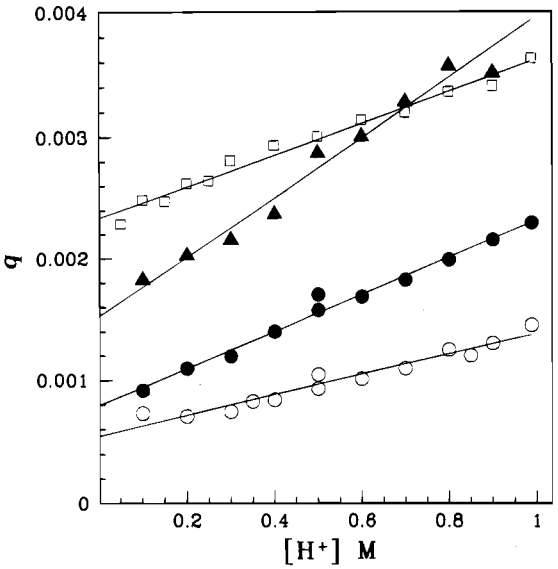

Figure 7. Initial-rate kinetic data for the slow step in the pH-jump dissociation of the iron(III) complexes with **IIIa**–**d**. The parameter q is defined in eq 20. $[Fe^{3+}]_{tot} = [L^{2-}]_{tot} = 0.30$ mM. $I = 2.0$ M ($NaClO_4/HClO_4$). $T = 25$ °C. $\lambda = 470$ nm. Data were analyzed using $q = a[H^+] + b$. Uncertainties quoted are 90% confidence limits. Key: (○) H_2L = **IIIa**, $a = 0.0008(1)$ M^{-1} s^{-1}, $b = 0.00055(7)$ s^{-1}; (●) H_2L = **IIIb**, $a = 0.0015(1)$ M^{-1} s^{-1}, $b = 0.00079(7)$ s^{-1}; (▲) H_2L = **IIIc**, $a = 0.0024(2)$ M^{-1} s^{-1}, $b = 0.0015(1)$ s^{-1}; (□) H_2L = **IIId**, $a = 0.0013(1)$ M^{-1} s^{-1}, $b = 0.00233(5)$ s^{-1}.

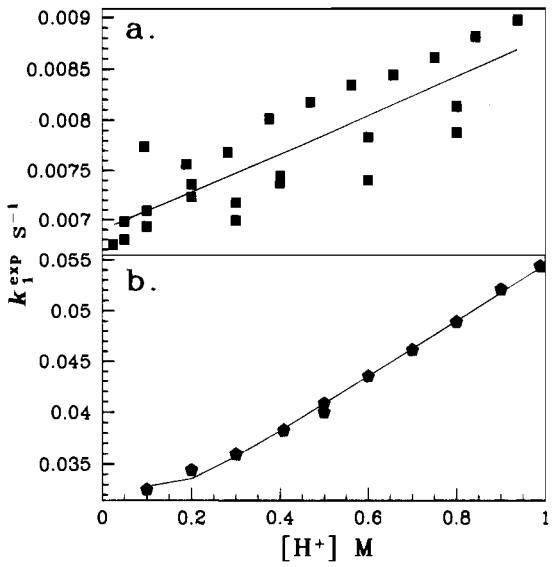

Figure 8. Kinetic data for the slow step in the pH-jump dissociation of the iron(III) complexes with **IIIe** and **IIIf**. $[Fe^{3+}]_{tot} = [L^{2-}]_{tot} = 0.30$ mM. $I = 2.0$ M ($NaClO_4/HClO_4$). $T = 25$ °C. $\lambda = 470$ nm. Data were analyzed using $k_1^{exp} = a[H^+] + b + c[H^+]^{-1}$. Key: (a) H_2L = **IIIe**, $a = 0.0019(4)$ M^{-1} s^{-1}, $b = 0.0069(2)$ s^{-1}, $c \approx 0$ M s^{-1}, $r^2 = 0.85$; (b) H_2L = **IIIf**, $a = 0.029(7)$ M^{-1} s^{-1}, $b = 0.026(6)$ s^{-1}, $c = 3.3 \times 10^{-4}$ M s^{-1}, $r^2 = 1.000$. Uncertainties quoted are 90% confidence limits.

Table 3. Microscopic Kinetic Parameters Defined in Scheme 3 for the Final Step in the Dissociation of (Dihydroxamato)iron(III) Complexes[a]

ligand	k_1[d]	k_{-1}[d,e]	k_1'[f]	$10^3k_{-1}'$[d,e]
IIIa[b]	0.0008(1)	40(40)	0.00055(7)	18(18)
IIIb[b]	0.0015(1)	8(4)	0.00079(7)	3(1)
IIIc[b]	0.0024(2)	3(1)	0.0015(1)	1.4(4)
IIId[b]	0.0013(1)	1.7(1)	0.00233(5)	2.0(1)
IIIe[c]	0.0019(4)	1.6(4)	0.0069(2)	3.8(6)
IIIf[c]	0.029(7)	1.7(5)	0.026(6)	1.0(3)

[a] $[Fe^{3+}]_{tot} = [L^{2-}]_{tot} = 0.30$ mM. $I = 2.0$ M ($NaClO_4/HClO_4$). $T = 25$ °C. Uncertainties quoted are 90% confidence limits. [b] Initial rate studies. Dissociation rate parameters determined from experimental data using eq 20. [c] Full rate analysis. Dissociation rate parameters determined from experimental data using eq 21. [d] M^{-1} s^{-1}. [e] Computed from equilibrium data, $k_r = k_f/K$. [f] s^{-1}.

relating k_1^{exp} to $[H^+]$ is eq 21. Because of the second-order

$$k_1^{exp} = k_{-1}'\beta_H[H^+]^{-1}([Fe^{3+}]_{tot} - [FeLH^{2+}]_{eq}) + k_1' + k_1[H^+] \quad (21)$$

nature of the reverse reactions in eqs 16–18, the term $[Fe^{3+}]_{tot} - [FeLH^{2+}]_{eq}$ is not strictly constant, as has been assumed in fitting eq 21 to the rate constant data for mono(hydroxamato)-iron(III) dissociation.[3,4,46] It has been pointed out, however, that it may be nominally constant for purposes of analyzing the kinetic data, insofar as accounting for variation in $[FeLH^{2+}]_{eq}$ does not seem to affect the values of the parameters k_1 and k_1'.[19] The microscopic rate parameters, k_1 and k_1', were determined by fitting eq 21 to the data in Figure 8. The rate constants k_{-1} and k_{-1}' for the reverse reaction were determined from equilibrium parameters (Table 1) and are listed in Table 3.

Mechanism of the Slow Step. The kinetic data obtained for the slow step are consistent with the dual-path mechanism for dissociation of $FeLH^{2+}$ illustrated in Scheme 3. This type of mechanism is observed for dissociation of monodentate and bidentate complexes of iron(III) with various ligands.[9] The fundamental difference between the two pathways is the source of the proton necessary for dissociation. The upper path involves an acid-dependent dissociation of one hydroxamate group to give the free iron(III) solution species, $Fe(OH_2)_6^{3+}$, where the proton is obtained from bulk solution. The lower path involves abstraction of a proton from a coordinated water by the ligand to yield the monohydroxide species $Fe(OH_2)_5OH^{2+}$ in solution. This occurs due to the higher acidity of the coordinated water relative to the protonated hydroxamate ligand. The two iron(III) product species are related by the protonation constant of iron(III) in 2.0 M $NaClO_4$ solution, $\beta_H = 1.51 \times 10^{-3}$ M.[53,54]

Discussion

Scheme 3, Fast Step (Paths 1 and 2). It is useful to make a few qualitative comparisons between the initial dissociation steps for some various known bis(hydroxamato)iron(III) systems, eqs 22–24 (HA = monohydroxamic acid, H_2L =

$$FeA_2^+ + H^+ \rightleftharpoons FeA^{2+} + HA \quad (22)$$

$$FeL^+ + H^+ \rightleftharpoons FeLH'^{2+} \rightleftharpoons FeLH^{2+} \quad (23)$$

$$FeH_2DFB^{2+} + H^+ \rightleftharpoons FeH_3DFB'^{3+} \rightleftharpoons FeH_3DFB^{3+} \quad (24)$$

dihydroxamic acid, H_4DFB^+ = deferriferrioxamine B). For the dissociation of the initial hydroxamate ligand from bis(hydroxamato)iron(III) complexes involving monohydroxamic acids HA, only a single step is kinetically observed for dissociation of the first hydroxamate group,[6,19] eq 22. However, the kinetic data for dissociation of bis(hydroxamato)iron(III) complexes can best be explained if the reaction occurs in two discrete steps: the fast initial cleavage of the Fe–O(N) bond followed by the rate-limiting cleavage of the Fe–O(C) bond.[3,4,6,19,46] For dissociation of the initial hydroxamate group from the mono-

(53) Milburn, R. M.; Vosburgh, W. C. *J. Am. Chem. Soc.* **1955**, *77*, 1352.
(54) Milburn, R. M. *J. Am. Chem. Soc.* **1957**, *79*, 537.

meric iron(III) complexes with **IIIa,b**, eq 23, an intermediate is kinetically observed and is interpreted to be a "half-opened" species $FeLH'^{2+}$, illustrated in Scheme 3. This tridentate-bonded complex, $FeLH'^{2+}$, is not observed as a stable intermediate for the monohydroxamic acid ligands HA.[6,19] In order to compare eq 23 to eq 22, we define an effective rate constant for eq 23:

$$k_{eff} = K_5 k_6 \tag{25}$$

The units of k_{eff} are M^{-1} s^{-1}. K_5 and k_6 for the monomeric (dihydroxamato)iron(III) complexes are listed in Tables 1 and 2. The values for k_{eff} for eq 23 are 0.21 and 83 M^{-1} s^{-1} for H_2L = **IIIa** and **IIIf**, respectively. On the other hand, the dissociation rate constants for eq 22 are 100 and 1400 M^{-1} s^{-1} when HA = *N*-methylacetohydroxamic acid[19] and acetohydroxamic acid,[6] respectively. The corresponding k_{eff} for eq 24, involving the tetradentate form of ferrioxamine B,[13,14] is 0.34 M^{-1} s^{-1} nearly identical to that for the iron(III) complex with **IIIa**. There is a general decrease in the effective dissociation rate constant by an order of magnitude or more when the two hydroxamate groups are part of the same ligand compared to an analogous complex in which the hydroxamate groups are independent. This may be ascribed to repulsive steric or hydrophobic effects on the incoming proton due to the presence of a bulky hydrophobic chain connecting the hydroxamate groups. This reduces the kinetic lability of the tetradentate-bound complexes with respect to proton-initiated dissociation.

A tridentate intermediate is observed in the dissociation of tetradentate ferrioxamine B,[13,14] FeH_2DFB^{2+}, illustrated in eq 24. This intermediate was intepreted to be a half-opened tridentate protonated complex, $FeH_3DFB'^{3+}$, analogous to the $FeLH'^{2+}$ complex in Scheme 3.[14] It seems apparent that the monomeric ferric dihydroxamate complexes, FeL^+, can function as a model for further elucidating the dissociation mechanism for ferrioxamine B. In addition, the complexes FeL^+ offer the opportunity to observe the tridentate Fe−O(C) coordination mode which exists only as an unstable transient for (monohydroxamato)iron(III) complexes.

Since removal of the second hydroxamate group from iron(III) in ferrioxamine B[13,14] is formally identical to removal of the first hydroxamate group from a monomeric ferric dihydroxamate complex, it is worthwhile to compare the mechanistic details of both. The fast step in the dissociation of the iron(III) complexes with **IIIa** and **IIIb** (Scheme 3 (path 1)) involves initial cleavage of the Fe−O(N) bond by H_3O^+, in which the proton enters prior to or simultaneously with Fe−O(N) bond breakage. The second step involves the acid-independent cleavage of the Fe−O(C) bond and substitution by H_2O. This is reminiscent of the general mechanism proposed for dissociation of iron(III)−monohydroxamic acid complexes, in which the Fe−O(N) and Fe−O(C) bonds are successively cleaved in a stepwise process requiring initial protonation of the oxime oxygen.[3,4,19,46]

A somewhat different mechanistic interpretation is required in the case of ferrioxamine B,[13,14] where there is a rapid pre-equilibrium step prior to removal of the second hydroxamate group. The pre-equilibrium is associated with the much faster removal of the first hydroxamate group from ferrioxamine B and is proton dependent.[13,14] However, cleavage of the second Fe−O(C) bond shows saturation kinetics in proton, so that the microscopic rate-limiting step must be proton independent.[13,14] The second proton must then enter after Fe−O(N) bond cleavage and is not associated with the bond-breaking process, as is the case for iron(III) complexes with **IIIa** and **IIIb**. Therefore, for removal of the second hydroxamate group from ferrioxamine B, the proton enters on the reaction coordinate later than for the model iron(III) dihydroxamate complexes.

The reason for this mechanistic difference is not clear. However, if the Fe−O(N) bond re-formation is rapid, then the dissociation reaction may require that the oxime oxygen be protonated in order to drive the dissociation reaction. If Fe−O(N) bond formation is slow, then Fe−O(C) bond cleavage may be able to take place more radily in the absence of protonation at the oxime site. Therefore, it may be suggested that a slower rate of Fe−O(N) bond formation in ferrioxamine B is partially responsible for the observed difference in proton dependence. This is in agreement with the larger Fe−O(N) formation rate constants for the iron(III) complexes of **IIIa** and **IIIb**, k_{-5} = 10−15 s^{-1}, compared to ferrioxamine B,[13,14] $k_{-5} \leq 3$ s^{-1}. It is possible that a slower rate of rotation about the hydroxamate C−N bond in ferrioxamine B has the effect of slowing down the Fe−O(N) formation rate,[19] due to the larger substituent attached to the hydroxamate nitrogen.

A single step is observed for the initial dissociation of the iron−**IIIc** system (Scheme 3 (path 1)). Therefore, an ambiguity exists in the assignment of the mechanistic details for this system. One possibility is that because of the added complexity of the additional second-order proton-dependent step, only one step of an actual two-step process can be observed. On the other hand, the shorter chain length induces strain in this system, which may increase the rate of Fe−O(C) cleavage. A significant increase in the rate of Fe−O(C) cleavage, k_6, will result in a lower time-dependent concentration of the tridentate intermediate, $FeLH'^{2+}$, provided the rate of Fe−O(N) cleavage has not been increased by an equivalent degree. The latter hypothesis is consistent with the 3−4-fold increase in k_6 and k_{-6} as n decreases from 8 (**IIIa**) to 7 (**IIIb**) and the nearly identical values for k_5 and k_{-5} for the same ligands.

The iron(III) complex with **IIIf** also exhibits a single observable reaction for the fast step. If the effective second-order rate constant for dissociation of the iron(III)−**IIIa** complex is K_5k_6 = 0.21 M^{-1} s^{-1}, then the overall second-order rate constant for dissociation of iron(III)−**IIIf**, k_2 = 83 M^{-1} s^{-1}, is 400 times as large. This increase in rate must be ascribed to the difference in R_N between **IIIa** and **IIIf**, since the two ligands are identical in other respects. The increase in rate is consistent with a decrease in electron density at the carbonyl oxygen of **IIIf** compared to **IIIa**, due to replacement of the electron-donating methyl group at the nitrogen site of **IIIa** by a poorly donating hydrogen atom.[2−4,19,20,46] The fact that no tridentate intermediate $FeLH'^{2+}$ (Scheme 3) is observed for **IIIf** suggests that, compared to that for **IIIa**, the rate of Fe−O(C) cleavage has been increased to a greater extent than the rate of Fe−O(N) cleavage, so that a lower concentration of the intermediate exists throughout the reaction. This is expected since substitution of H for methyl at the R_N site should weaken the Fe−O(C) bond more than the Fe−O(N) bond.

Scheme 3, Fast Step (Path 3). The presence of the dimer $Fe_2L_2^{2+}$ for small n is supported by kinetic data in this study and by electrospray mass spectrometric studies.[36,37] The $Fe_2L_2^{2+}$ complex is, in some ways, analogous to the neutral Fe_2L_3 complex believed to be relevant in iron transport in *Rhodotorula pilimanae*.[1,22−24] It is then useful to make some comparisons between the two structures.

The driving force leading to formation of $Fe_2L_2^{2+}$ is not the same as that driving formation of Fe_2L_3. The pH-independent and ligand-independent dimerization of FeL^+, eq 26, is driven

$$2FeL^+ \rightleftharpoons Fe_2L_2^{2+} \tag{26}$$

by the increasing steric strain in the monomeric complex with

Chart 1. Possible Structures for the Neutral Fe_2L_3 Complex[a]

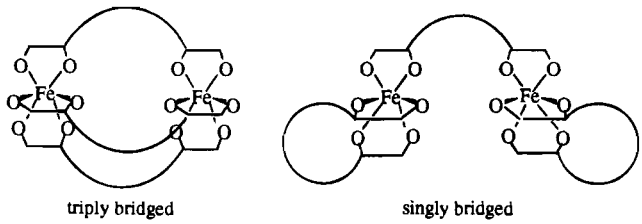

[a] Orientation of the hydroxamate groups is not shown.

decreasing n.[36,37] As n decreases, the ligand backbone is forced into an increasingly strained conformation in order to form the monomeric complex. Computations of relative steric energies for the monomeric and dimeric complexes for **IIIa** and **IIIc−e** suggested that the significant conformational strain for the short-chain ligands can be relieved if the system is allowed to dimerize.[37] The driving force for the pH-dependent ligand-dependent formation of Fe_2L_3, eq 27, is the strong enthalpic

$$2FeL^{2+} + H_2L \rightleftharpoons Fe_2L_3 + H^+ \qquad (27)$$

favorability for forming six-coordinate (hydroxamato)iron(III) complexes at pH > 3. Because a single ligand cannot satisfy a six-coordinate geometry, the strong affinity of hydroxamate groups for iron induces formation of the bimetallic Fe_2L_3 when the ligand is in at least a 1.5-fold excess over iron(III).

The structural difference between $Fe_2L_2^{2+}$ and Fe_2L_3 is in the presence of one additional dihydroxamate ligand, L^{2-}, in Fe_2L_3. There is some uncertainty as to whether the Fe_2L_3 complex is a singly-bridged or triply-bridged structure (Chart 1).[18,27,30] Since the $Fe_2L_2^{2+}$ dimeric complex existing for $n \leq 6$ must be doubly-bridged, the Fe_2L_3 complex is most likely triply-bridged for $n \leq 6$. This suggests, but does not confirm, that Fe_2L_3 is also triply-bridged for $n > 6$. Since a single ligand is flexible enough to bind a single iron for $n > 6$,[37] the singly-bridged structure in Chart 1 is still possible for the longer chain ligands.

A problem in the elucidation of the mechanism for protonation of $Fe_2L_2^{2+}$ is the multiplicity of protonation sites. All of the protonation sites on $Fe_2L_2^{2+}$ are equivalent, so that only one product can result from single protonation. However, the intermediate $Fe_2L_2H^{3+}$ has three nonequivalent protonation sites. Consequently, three possible products exist for protonation of $Fe_2L_2H^{3+}$ (Scheme 4). We can immediately reject protonation leading to **A** since dissociation will be much more rapid at the bis(hydroxamato)iron(III) center than at the mono(hydroxamato)iron(III) center of $Fe_2L_2H^{3+}$.[6,19] There is precedence for believing that the two proximal iron(III) sites are noninteracting,[27] at least for chain lengths n greater than 3 carbons. On the basis of this assumption, the dimeric complexes in Scheme 4 have been represented as having separate and independent charges on each iron center. We might, therefore, expect **B** to be less stable than **C** due to the added electrostatic repulsion of the two like charges in **B**. However, it is possible that **B** is the kinetically preferred species even though it may be thermodynamically less stable than **C**. Since neither the rate law nor the spectra will distinguish **B** and **C** under our conditions, an electrostatic model will be presented to suggest indirectly that the important species in Scheme 4 is **C**.

If a model for the intermediate $Fe_2L_2H^{3+}$ is assumed in which the 1+ and 2+ charged centers are independent and noninteracting, then Coulomb's law suggests an electrostatic contribution to the activation barrier for dissociation of $Fe_2L_2H^{3+}$, eq 28, in addition to the intrinsic barrier for dissociation of a general bis(hydroxamato)iron(III) complex. ΔE is the electrostatic repulsion that the incoming proton experiences from the 2+-charged iron center as it approaches the 1+ iron center. Formally, it is the work required to increase the charge on a point from 1+ to 2+ in the presence of a second 2+ charge. The distance separating the charged centers is r and the dielectric shielding constant is ϵ.

$$\Delta E = \frac{(2+)(2+)e^2}{\epsilon r} - \frac{(2+)(1+)e^2}{\epsilon r} = \frac{2e^2}{\epsilon r} \qquad (28)$$

The intrinsic contribution depends only on the nature of the metal and the binding site, so for our series of analogous dimeric complexes, the intrinsic contribution should be constant. Therefore, the activation barrier in kJ/mol, $\Delta G^{\ddagger}$, for dissociation of $Fe_2L_2H^{3+}$ can be broken down into two major contributions, eq 29: an intrinsic contribution $\Delta G^{\ddagger}_{int}$, and that due to the additional electrostatic repulsion, given by Coulomb's law. If

$$\Delta G^{\ddagger} = \frac{2e^2NC}{\epsilon r \times 10^{-8}} + \Delta G^{\ddagger}_{int} \qquad (29)$$

e = electrostatic charge = 4.80×10^{-10} esu

N = Avogadro's number = 6.02×10^{23}

$C = 1 \times 10^{-7}$ J/erg

r = Fe−Fe separation in angstroms

the rate constant for dissociation of $Fe_2L_2H^{3+}$ is k_3, then we can convert from kJ/mol into ln k_3 units by dividing both sides by $-RT$. This yields a theoretical equation relating the rate constant ln k_3 to r:

$$\ln k_3 = -1.1 \times 10^3\left(\frac{1}{\epsilon r}\right) + \ln k_{3(int)} \qquad (30)$$

According to eq 30, if ln $k_{3(int)}$ is a constant, then ln k_3 should vary linearly with respect to $1/r$ with a slope of $(-1.1 \times 10^3)/\epsilon$. Conformational analysis has been performed by computation of relative steric energies for the dimeric iron(III) complexes $Fe_2L_2^{2+}$, H_2L = **IIIc−e**.[37] These calculations gave the lowest energy conformation of the dimeric complex, from which average inter-iron distances r for $Fe_2L_2^{2+}$ are estimated to be 11.0, 8.2, and 5.5 Å for the dimeric complexes with **IIIc−e**, respectively.[55] Reliable estimates for r could not be obtained by direct conformational analysis of $Fe_2L_2H^{3+}$ due to the multiplicity of stable conformations having comparable energies. The values of k_3 are given in Table 2 for **IIIc−e**.

Plotting ln k_3 against $1/r$ (Figure 9), the expected trend for ln k_3 to decrease as r decreases is confirmed. The value of ln k_3 at the point at which $1/r = 0$ is defined as the intrinsic activation barrier since $r = \infty$ at this point, and the electrostatic contribution from the second charged site is zero. The dissociation of bis(*N*-methylacetohydroxamato)iron(III),[19] $Fe(NMHA)_2^+$, is used as a baseline system for defining ln $k_{3(int)}$ since $Fe(NMHA)_2^+$ is a monomeric complex whose iron binding site is identical to that for our model dihydroxamate complexes.[19] Therefore, the only contribution to the activation barrier in $Fe(NMHA)_2^+$ is the intrinsic contribution.

The plot in Figure 9 is not strictly linear as predicted by eq 30. However, the first three points may lie on a straight line with a slope of -15 Å^{-1}. If all four points are used, the slope

(55) For a more detailed explanation of the molecular mechanics calculations used to estimate the most stable conformations, see ref 37.

Scheme 4. Possible Pathways for the Protonation of $Fe_2L_2H^{3+}$

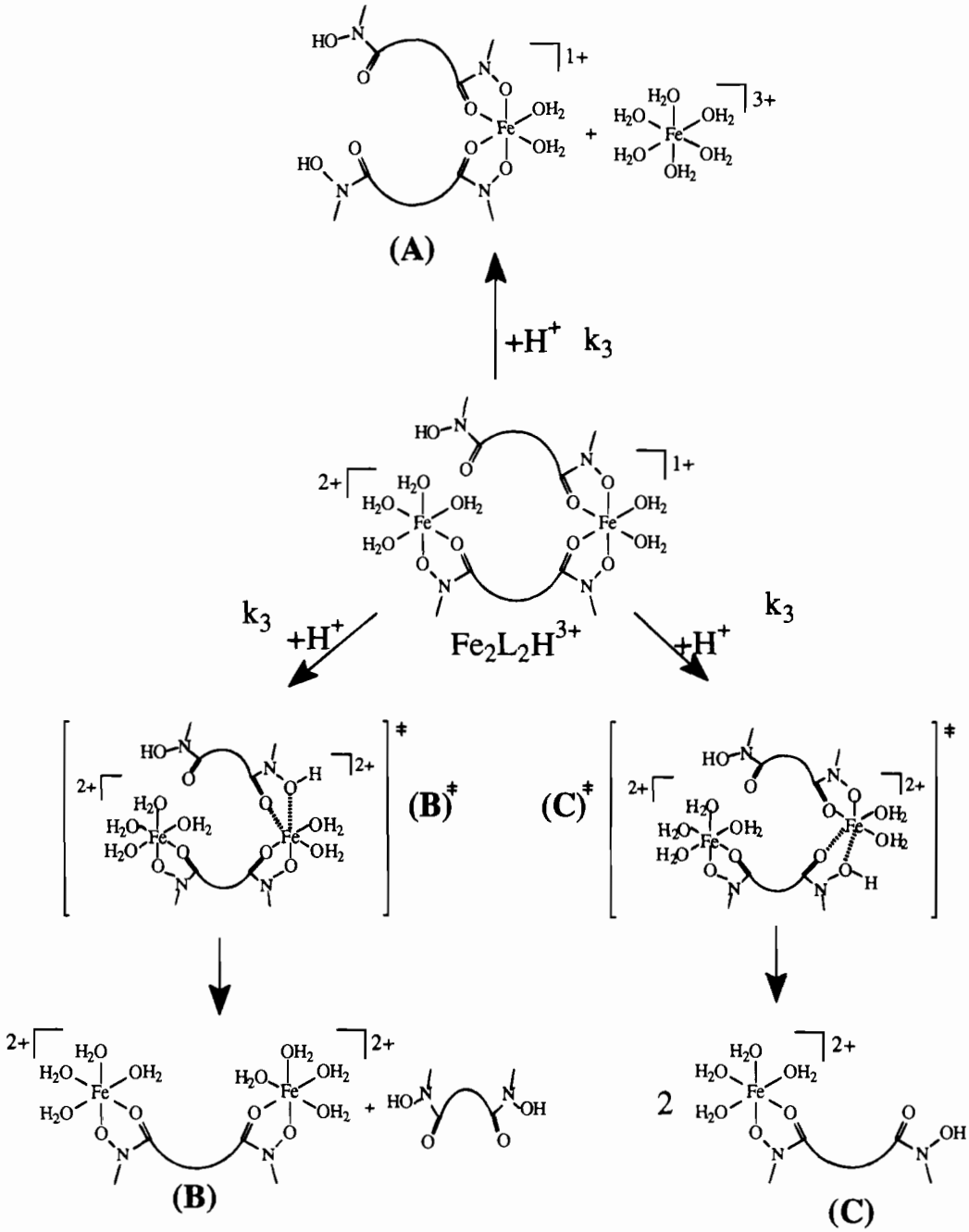

becomes -22 Å^{-1}. A comparison of the actual slopes in Figure 9 with the theoretical expression for the slope in eq 30 allows us to estimate ϵ. For the maximum and minimum slope values of -22 and -15 Å^{-1}, we compute a dielectric constant for the system of between 50 and 73. These values are quite reasonable, and the value computed using only the first three points is close to the bulk dielectric constant of water, 78.54.[56] This agreement may be fortuitous, however, since the bulk (or continuum) dielectric constant of water may not be applicable on the noncontinuum intramolecular scale of relevence here. Also, a large part of the dielectric shielding between the two iron(III) centers in $Fe_2L_2H^{3+}$ is probably due not to water but to electron density on atoms within the complex itself, *i.e.* the ligand backbone. In any event, the simple electrostatic model for protonation of $Fe_2L_2H^{3+}$ is at least in qualitative if not quantitative agreement with our experimental results.

The nonlinearity in the plot presented in Figure 9 is introduced by limitations in the simple electrostatic model. Effects such as entropy effects associated with the various chain lengths, variations in ϵ with n, and solvent cage effects are not accounted for. One additional factor not included in eq 30 is the possibility of electronic coupling interactions between the two iron centers, particularly at small n.[27] In fact, the derivation of eq 30 assumes there is no such coupling. However, it has been predicted that spin–spin interactions are possible, though not required, when an Fe–Fe distance is less than about 9 Å.[57] The Fe–Fe distance is estimated by our calculations to be 5.5 Å in the iron(III)–**IIIe** dimeric system and only 8.2 Å in the **IIId** dimer system.[37] These are both within the range where Fe–Fe interactions are possible.[57] If an electronic coupling interaction were to occur between the irons, then this might be expected to slow the rate of dissociation due to (1) the incipient bond formation between

(56) Lide, D. R., Ed. *CRC Handbook of Chemistry and Physics*, 73rd ed.; CRC Press, Inc.: Ann Arbor, MI, 1992–1993.

(57) Aasa, R.; Malmström, B. G.; Saltman, P.; Vannagard, T. *Biochim. Biophys. Acta* **1963**, *75*, 203.

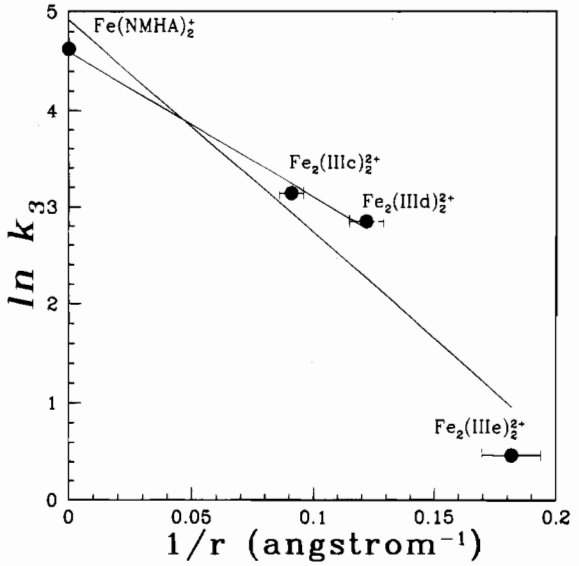

Figure 9. Dependence of ln k_3 and r. Rate constants k_3 are taken from Table 2 for **IIIc−e** and from ref 19 for NMHA. The average inter-iron distance for a given complex $Fe_2L_2H^{3+}$ was estimated to be equivalent to that in $Fe_2L_2^{2+}$. The inter-iron distance in $Fe_2L_2^{2+}$ was determined from molecular mechanics conformational studies on the dimeric complexes with ligands **IIIc−e**.[37] Error bars show estimated uncertainty in $1/r$, ≈90% confidence interval. Using the first three points, slope = −15, intercept = 4.6, and r^2 = 0.99. Using all of the points, slope = −22, intercept = 5, and r^2 = 0.96. $[Fe^{3+}]_{tot} = [L^{2-}]_{tot}$ = 0.30 mM. I = 2.0 M ($NaClO_4$/$HClO_4$). T = 25 °C.

the two metal centers and (2) the charge equalization effect which may give the bis(hydroxamato)iron(III) center in $Fe_2L_2H^{3+}$ a partial charge higher than 1+.

The effects just discussed consider only the process leading to initial protonation of the complex and the related energetic factors. There is still the issue of where on the bis(hydroxamato)iron(III) center of $Fe_2L_2H^{3+}$ the protonation takes place and which species in Scheme 4, **B** or **C**, results from the dissociation reaction. This question is equivalent to asking which metal−ligand bonds are likely to be broken in the transition state for the dissociation of Fe_2L_2H.

It has been shown that, for dissociation of tris-, bis-, and mono(hydroxamato)iron(III) complexes, a late transition state, in which the metal−ligand bonds are largely broken, is most consistent with experimental observations.[19] If we consider the dissociation process after the initial protonation of the complex (Scheme 4), two possibilities for the transition state structure present themselves: $\mathbf{B}^{\ddagger}$ and $\mathbf{C}^{\ddagger}$, for the transition state leading to **B** and **C**, respectively. The kinetically more favored pathway will involve the transition state having the relatively lower energy. In $\mathbf{B}^{\ddagger}$ the neutral ligand leaving group has largely dissociated, leaving whatever partial part of the 2+ charge it carried on the iron center from which it dissociated. However, the two iron centers are constrained to remain the same distance apart in $\mathbf{B}^{\ddagger}$, so that no attenuation of the electrostatic repulsion is possible. In fact, if the 2+ charge is more localized on the iron center in $\mathbf{B}^{\ddagger}$ than on that in $Fe_2L_2H^{3+}$, then the electrostatic repulsion between the iron centers will be higher in the transition state than in the ground state. A consideration of the transition state $\mathbf{C}^{\ddagger}$ would suggest that the electrostatic repulsion should be less than for $\mathbf{B}^{\ddagger}$. In $\mathbf{C}^{\ddagger}$, it is the charged iron center which is dissociating from the complex, allowing it to move further away from the second iron while still in the transition state. This places it further from the proximal 2+ charge and reduces the electrostatic repulsion between the iron centers compared to that in $\mathbf{B}^{\ddagger}$. Therefore, electrostatic arguments suggest that $\mathbf{C}^{\ddagger}$ is a somewhat lower energy pathway for the dissociation of $Fe_2L_2H^{3+}$ which, in turn, suggests that the important dissociation product in consideration of Scheme 4 is **C**.

Scheme 3, Slow Step. The dissociation reaction of mono(hydroxamato)iron(III) complexes is the most extensively studied mechanistic aspect involving the iron(III) solution reactions with hydroxamic acids.[3−17] The mechanism for removal of the final hydroxamate group has been fairly well established to be that illustrated in Scheme 3.[2−4,9,14,15,19,46] This mechanism has, in fact, been shown to be applicable to iron(III) complex dissociation reactions in general.[9]

The average k_{-1}'/k_{-1} ratio (Table 3) is 905, meaning that the replacement of two water molecules by a single bidentate hydroxamate group is, on average, 900 times faster for $Fe(OH_2)_5OH^{2+}$ than for $Fe(OH_2)_6^{3+}$. The ratio is consistent with that for water exchange rate constants on the same species, 750.[58] This suggests that the rate-limiting step in ligand substitution by a dihydroxamate ligand is mechanistically related to water exchange. Volume and entropy of activation studies show that, for water exchange, there is a shift from associative activation for $Fe(OH_2)_6^{3+}$ to more dissociative character for $Fe(OH_2)_5OH^{2+}$.[59] A similar shift in activation mode has been proposed for formation of mono(hydroxamato)iron(III) complexes *via* $Fe(OH_2)_6^{3+}$ and $Fe(OH_2)_5OH^{2+}$.[3−5,19,46,60]

For dissociation or aquation mechanisms having acid-dependent and -independent steps (Figure 10 (top)) whose transition states differ only by the presence of a proton, a theoretical basis for a linear relationship between ln k_1 and ln k_1' has been described.[60,61] A simplified statement of this relationship is given in eq 31. K_t is defined by eq 32, where

$$\ln k_1 = \ln k_1' + \ln K_t \tag{31}$$

$$-\ln K_t = \frac{\Delta G_t^{\ddagger}}{RT} \tag{32}$$

$\Delta G_t^{\ddagger}$ is the free energy difference between the two transition states shown in Figure 10 (top). On the basis of eq 32, one may consider K_t to be the "protonation constant" for the transition state. Provided K_t is constant, a plot of ln k_1 against ln k_1' will be linear with unit slope. It has been established that, for the dissociation of a large series of mono(hydroxamato)iron(III) complexes, the transition state energies for the acid-dependent and acid-independent dissociation of bidentate (hydroxamato)iron(III) complexes (Figure 10) are correlated in this way. Figure 10 illustrates this correlation,[3,4,15,46] including the current set of bidentate coordinated (dihydroxamato)iron(III) complexes. $FeLH^+$ (H_2L = **IIIa−f**). The rate constant ln k_1 is linearly related to ln k_1' as suggested by eq 31, although there is scatter in the data. The actual slope of 0.9(1) is within experimental error equal to the theoretical value of unity. From the intercept of this plot containing a variety and range of hydroxamate and thiohydroxamate ligands,[3,4,15,46] we find ln K_t = −0.6. Therefore, $\Delta G_t^{\ddagger}$ is small, 3 kJ/mol or less, and constant for this entire series of hydroxamic acids. The fact that $\Delta G_t^{\ddagger}$ is invariant with ligand is not surprising since the transition states (Figure 10 (top)) differ only by the presence of a single proton. Since the acidity of the hydroxylamino site in hydroxamic acids does not vary in any large or systematic way with the structure of the ligand,[62−65] we should expect that

(58) Grant, M.; Jordan, R. B. *Inorg. Chem.* **1981**, *20*, 55.
(59) Swaddle, T. W.; Merbach, A. E. *Inorg. Chem.* **1981**, *20*, 4212.
(60) Crumbliss, A. L.; Garrison, J. M. *Comments Inorg. Chem.* **1988**, *8*, 1.
(61) Asher, L. E.; Deutsch, E. *Inorg. Chem.* **1973**, *12*, 1774.
(62) Monzyk, B.; Crumbliss, A. L. *J. Org. Chem.* **1980**, *45*, 45.
(63) Brink, C. P.; Crumbliss, A. L. *J. Org. Chem.* **1982**, *47*, 1171.
(64) Brink, C. P.; Fish, L.; Crumbliss, A. L. *J. Org. Chem.* **1985**, *50*, 2277.

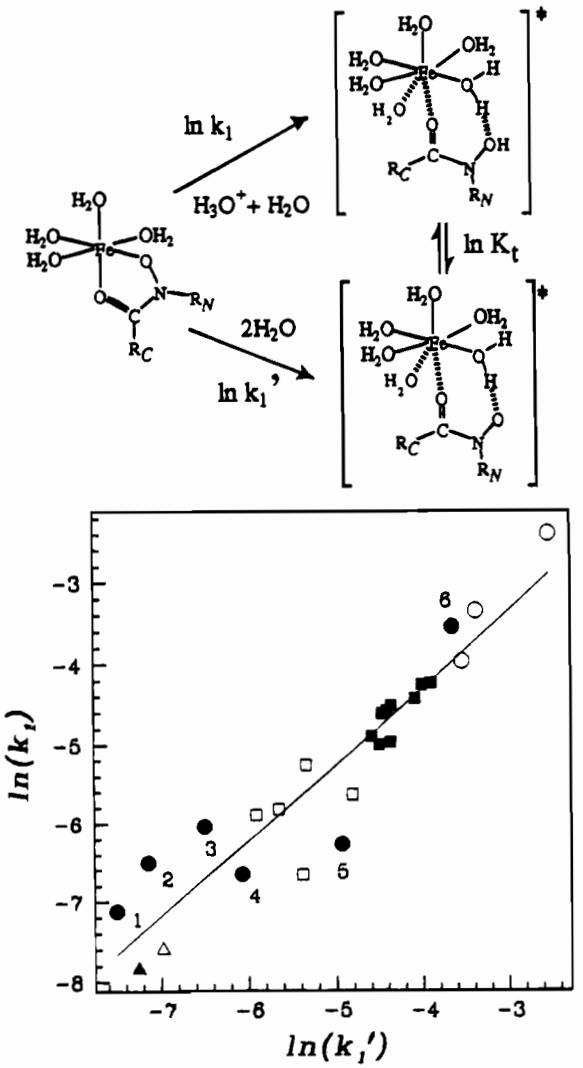

Figure 10. Top: Transition states for dual-path dissociation of (monohydroxamato)iron(III) complexes; charges omitted for clarity. Bottom: Plot of ln k_1 *vs* ln k_1' for the dissociation of bidentate (monohydroxamato)iron(III), (dihydroxamato)iron(III), and (trihydroxamato)iron(III) complexes. I = 2.0 M ($NaClO_4/HClO_4$). T = 25 °C. Slope = 0.9(0.1); intercept = −0.6(7); s_y = 0.47; r^2 = 0.92. Uncertainties quoted are 90% confidence limits. ● = bidentate-(dihydroxamato)iron(III) complexes from this study (Table 3): 1, **IIIa**; 2, **IIIb**; 3, **IIIc**; 4, **IIId**; 5, **IIIe**; 6, **IIIf**. □ = *N*-methyl-substituted (monohydroxamato)iron(III) complexes.[3,4] ■ = *N*-phenyl-substituted (monohydroxamato)iron(III) complexes.[3,4] ○ = unsubstituted (monohydroxamato)iron(III) complexes.[3,4] ▲ = bidentate ferrioxamine B.[13] △ = $Fe(HN(O)C(S)C_6H_4OCH_3)^{2+}$.[46]

protonation of the transition state (at the hydroxylamino site) leading to dissociation would show little dependence on the nature of the ligand.

Mechanistic similarity between each step in the acid-dependent dissociation of tris-, bis-, and mono(hydroxamato)-iron(III) complexes has been established by observing a common linear correlation between the activation barrier and the equilibrium constant for the dissociation of multiple *different* hydroxamate ligands from iron(III).[19] This correlation has been extended here to include the current bidentate dihydroxamate complexes $FeLH^{2+}$, H_2L = **IIIa**−**f** (Figure 11). The theoretical basis for constructing such a plot has been presented.[19] The important feature in Figure 11 is the high degree of correlation between the equilibrium constant for dissociation and the rate

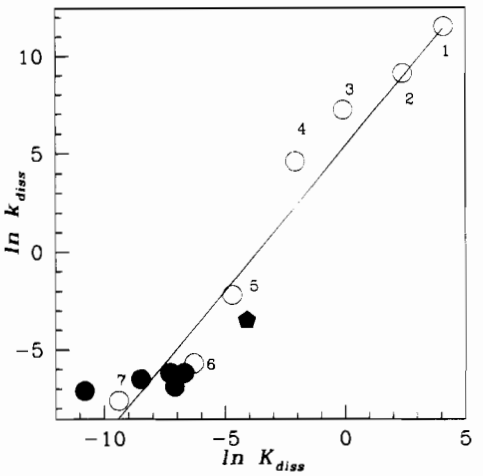

Figure 11. Plot of ln k_{diss} *vs* ln K_{diss} for tris-, bis-, and mono-(hydroxamato)iron(III) dissociation reactions including reactions of bidentate (dihydroxamato)iron(III) complexes $FeLH^{2+}$. I = 2.0 M ($NaClO_4/HClO_4$). T = 25 °C. Slope = 1.5(2); intercept = 5(1); s_y = 1.9; r^2 = 0.96. Uncertainties quoted are 90% confidence limits. AHA = acetohydroxamate anion, data from ref 6. NMHA = *N*-methylacetohydroxamate anion, data from ref 19. H_3DFB = bidentate ferrioxamine B ligand, data from ref 13. ○: 1, $Fe(AHA)_3$; 2, $Fe(NMHA)_3$; 3, $Fe(AHA)_2^+$; 4, $Fe(NMHA)_2^+$; 5, $Fe(AHA)^{2+}$; 6, $Fe(NMHA)^{2+}$; 7, FeH_3DFB^{3+}. ● = bidentate complexes $FeLH^+$, H_2L = **IIIa**−**e**, this work (Tables 1 and 3; $k_{diss} = k_1$, $K_{diss} = K_1$). ● = bidentate complexes $FeLH^+$, H_2L = **IIIf**, this work (Tables 1 and 3; $k_{diss} = k_1$, $K_{diss} = K_1$).

constant for the same process. Such high correlation implies a minimal role for the ligand in the transition state. However, for complete correlation between the transition state and the products, where the ligand plays no role in the transition state, the slope in Figure 11 should be unity. The deviation from unity in Figure 11, slope = 1.5, is intepreted to mean that the ligand does, in fact, play a small role in the transition state.[19] Figure 11 then implies a late transition state for the dissociation reaction coordinate where the metal−ligand bonds are largely but not completely broken.

Since all of the data in Figure 11 lie on the same correlation, this suggests that the final step in the dissociation of ferric dihydroxamate complexes reported here is mechanistically similar to all three dissociation steps of the iron(III) complexes with monohydroxamic acids and is mechanistically similar to the final step in the dissociation of ferrioxamine B. Such mechanistic similarity is supported by Figure 10 as well, where a linear correlation is observed only if K_t is constant for a series of complexes. Since Fe−O(C) bond cleavage is believed to be rate limiting for dissociation of the model (monohydroxamato)iron(III) complexes,[2-4,19,46] Figures 10 and 11 suggest that the same is true for the bidentate-bound dihydroxamate complexes reported here and for the natural siderophore system ferrioxamine B.

Summary and Conclusions

One of the major problems in iron transport systems is the mechanism by which iron is removed from the extremely stable siderophore complex.[1,2] Since the dihydroxamic acids we have studied can be used as mimics or models for siderophore ligands, mechanistic information gathered for the model (dihydroxamato)iron(III) systems should be very useful in elucidation of the details of iron release. We have shown that the dissociation of the longer chain model dihydroxamic acid ligands, $n \geq 6$, occurs in a way largely analogous to the dissociation of ferrioxamine B,[13,14] in spite of some subtle mechanistic differences. In particular, we have shown that the same intermediates

(65) Ventura, O. N.; Rama, J. B.; Turi, L.; Dannenberg, J. J. *J. Am. Chem. Soc.* **1993**, *115*, 5754.

are involved in the dissociation of the long-chain model tetradentate (dihydroxamato)iron(III) complexes as are involved in the dissociation of tetradentate ferrioxamine B. Furthermore, the chain length is a very important factor in consideration of the structural features of siderophores. Hydroxamate siderophore ligands have more than six atoms separating the hydroxamate sites.[20,21] The kinetic data presented here on model iron(III) dihydroxamates show that this is a requirement in order to efficiently form a monomeric complex.[37]

We also elucidated the role of electrostatics in control of the dissociation of dimeric ferric dihydroxamate complexes. The dissociation rate slowed as the number of methylene groups n separating the binding sites decreased, that is, as the two charged iron(III) centers in the intermediate $Fe_2L_2H^{3+}$ are placed in closer proximity. This suggests a secondary role played by the $-NH_3^+$ group in ferrioxamine B. In addition to having a solubilizing effect, it may have the effect of repelling the incoming proton, making the entire complex more substitutionally inert with respect to proton-initiated ligand exchange.

Finally, the kinetic approach to the problem of (dihydroxamato)iron(III) dissociation and coordination chemistry illustrates an unusual case where equilibrium studies give at best incomplete information about the system and, at worst, erroneous information on the species existing in solution. The monomer−dimer nature of the 1:1 iron(III) dihydroxamate systems studied here was proposed on the basis of detailed kinetic evidence, which was confirmed by independent mass spectrometric studies.[36,37] Therefore, this work is an example of the degree of detail available from kinetic studies that is not available from equilibrium-based studies alone on iron siderophore and model siderophore systems.

Acknowledgment. We are grateful for the support of the donors of Petroleum Research Fund, administered by the American Chemical Society, and the National Science Foundation (Grant CHE-9112199). We also thank Dr. Frédérick Chaubet for assistance with initial ligand syntheses.

Supplementary Material Available: A proof that the dependence of the absorption spectrum (per iron center) on the protonation state of the iron complex will be identical for monomer **a** and dimer **b** in Scheme 2 and a derivation of the functions q used in analysis of the initial rate kinetic data for the slow final dissociation step (9 pages). Ordering information is given on any current masthead page.